ABSTRACT

NACKATHAYA, DILEEP BALAKRISHNA. Direct Numerical Simulation of Premixed Flame Kernel Ignition of Hydrogen-Air Mixtures under Turbulent Conditions. (Under the direction of Dr. Tarek Echekki.)

The role of turbulence conditions on the initial and subsequent stages of premixed flame kernel formation during the ignition of hydrogen-air mixtures is studied using Direct Numerical Simulation (DNS). Simulations are done using the Pencil code, an open-source code for DNS of compressible turbulent reactive flows. A six-step reduced mechanism for hydrogen-air combustion, and detailed thermal and mass transport formulations are used for the test-cases, along with third-order Runge-Kutta time-stepping and a sixth-order spatial discretization scheme. Navier-Stokes Characteristic Boundary Conditions (NCSBC) are used for treatment of solution at the boundaries.

Runs are made at two different turbulence intensities for each of the two different turbulence length scales. The results are compared with a reference case with no turbulence or mean-flow. It is found that small-scaled and more intense turbulence initially inhibits, but later enhances kernel growth, as against the other cases of turbulence, which exhibit similar trends as the laminar kernel, during the early stages of kernel evolution. At a given turbulence intensity, decreasing the characteristic turbulence length scale, enhances the burning intensity of the fuel; similar behavior is observed when turbulence intensity is increased at a fixed turbulence length scale. The highest enhancement was observed for the case with the lowest length scale and the highest intensity of turbulence. Higher wrinkling of the flame surface, and thus higher strain rates, was observed for lower length scales and

higher intensities of turbulence, signifying the importance of the nature of turbulent structures on chemistry and surface statistics of premixed flame kernels.

Direct Numerical Simulation of Premixed Flame Kernel Ignition of Hydrogen-Air Mixtures under Turbulent Conditions

by
Dileep Balakrishna Nackathaya

A thesis submitted to the Graduate Faculty of
North Carolina State University
in partial fulfillment of the
requirements for the degree of
Master of Science

Mechanical Engineering

Raleigh, North Carolina

2012

APPROVED BY:

Dr. Alexei Saveliev

Dr. Tiegang Fang

Dr. Tarek Echekki
Chair of Advisory Committee

DEDICATION

This thesis is dedicated to my father, Balakrishna Nackathaya, and to my mother, Suprasanna Nackathaya for their unconditional love, unending support and unquestioning faith in my abilities and decisions. They have lived lives that I aspire to and have led me by example. If I have any good in me, it is because of them.

BIOGRAPHY

Dileep Balakrishna Nackathaya was born on November 15th, 1988 in Udupi, a coastal town in the southwestern part of Karnataka, India. He obtained his Bachelor of Engineering Degree from S.D.M College of Engineering and Technology, affiliated to Visveswaraya Technological University, Karntaka in June 2010. After graduating, he started his graduate work at North Carolina State University towards Master of Science in Mechanical Engineering.

ACKNOWLEDGEMENTS

I would like to place on record, my heartfelt thanks to my advisor, Dr. Tarek Echekki. He has been extremely helpful and very patient with me. Working on this project has been a great learning experience, full thanks for which should go to him. I would also like to thank Dr. Alexei Saveliev and Dr. Tiegang Fang for their help and for serving as my committee members. Many thanks are also due to Dr. Axel Brandenburg and Dr. Nils Haugen for providing me with the Pencil code and for being kind enough to clarify my doubts regarding the code.

Furthermore, I would like to thank my labmates, Sami, Fu, Andreas, Hessam and Hamed for their help and for making work more enjoyable. Sami and Fu, thank you for your friendships; you rock!

Special thanks to my chums, Abhi, Dr. Raj, Uncle, Gupta, Bihari, Malladi, Laddoo, Silpakka, Jassi and Sriki (not necessarily in that order) for making my stay at N.C State terrific and leaving me with some of the best memories of my life. They have, in many ways, made me a better person. Cheers! When I found myself in the midst of hopelessness and gloom, Kitty, Mummy, Didi, Aniswa and Deepsali provided me a shelter and kept me going. I simply cannot thank them enough. I would like to take this opportunity to thank two special individuals, my late uncle, Dr. Murari Ballal, who taught me what life was all about, and my uncle, Dr. Bharath Ballal for introducing me to the joy of learning and doing science. Lastly, none of this would be possible without the love and support of my brother, Manu, my grandparents, uncles, aunts, and cousins, especially Siddharth.

TABLE OF CONTENTS

LIST OF TABLES

LIST OF FIGURES

CHAPTER 1

Introduction

In this chapter, the motivation for conducting this study and the objectives of the study are discussed. Relevant literature is reviewed, and the outline for the thesis is presented.

1.1 Motivation

Fossil-fuel combustion is currently the primary source of energy in the world. Therefore, there is a growing need to mitigate pollutant emissions from combustion sources. Such an effort would entail the understanding of the fundamental nature of interactions between turbulence and chemistry. A Premixed flame kernel configuration under turbulent conditions allows the study of the effects of turbulence scales and intensity on the fate and nature of flame-fronts, which is crucial to the development of premixed flame models and combustion device developments [3]. Premixed combustion of hydrogen in air has received renewed interest of late. This may be attributed to the fact that hydrogen energy has some interesting properties, namely, clean burning, higher laminar flame speed, lower lean flammability limit and greater resistance to strain and extinction [2, 3]. An important challenge in designing combustion devices is maintaining stable combustion, since combustion devices are prone to a number of instabilities that arise due to the combustion process. It has been found that for premixed combustion of hydrogen in air, the neutral stable flame is at equivalence ratios in the range 0.6 to 0.7. Preferential diffusion effects are known to occur in the flame for equivalence ratios outside this range. The selection of a

stoichiometric mixture of hydrogen an air is useful for the study of preferential diffusion instabilities. Studying these instabilities is the first step in the development of strategies to mitigate them. The fate of a kernel under turbulent conditions is decided by the initial stages of its development. Studying these initial stages is thus of great importance. Having an initial temperature profile, as against a flame kernel, helps in the understanding of the effect turbulence has on ignition delay and the initial stages of evolution of the flame kernel. Having cases with different characteristic length scales and intensities of turbulence allows for the study of interactions between flame fronts and turbulent eddies, and the effect the sizes and strengths of these eddies have on the shape and development of flame kernels.

Since direct numerical simulation (DNS) solves the complete system of Navier-Stokes equations, and resolves all the length and time-scales, there is no need for closure models and simplifications. Results from DNS with realistic models for chemistry and detailed multi-component diffusion transport, thus are very good representatives of the actual physics of the system at hand. Due to its high resolution, DNS also allows the study of transient statistics of the flame kernel. However, the current applications of DNS are limited to laboratory-type problems. Using DNS for complex real-world problems is prohibitively expensive with the existing state of the art. Due to the relative simplicity of Hydrogen reaction mechanisms, the choice of DNS for the study of ignition in hydrogen-air mixtures in isotropic turbulence is appropriate. This simplicity also enables conducting simulations in three dimensional domains without very large demands for computational resources and time. Further, the availability of open-source codes for DNS of turbulent reactive flows and post-processing of

results from such simulations makes conducting studies of this nature convenient and relevant.

1.2 Literature Review

A few studies have been made on the early stages of ignition of premixed hydrogen-air kernels under turbulent conditions using DNS. Experimental studies of early stages of ignition are extremely rare due to practical difficulties associated with conducting such a study. However, a number of studies have been made on the later stages of flame kernel evolution and fully-developed flames. The development of faster processors and larger storage devices has rekindled interest in DNS of turbulent reactive flows. Studies of turbulent combustion with detailed chemistry and transport in three-dimensional domains using DNS have seen a considerable increase in number of late. The use of Pencil code for DNS of turbulent combustion of hydrogen-air mixtures was shown by Babkovskaia et al. [1] with realistic chemistry and detailed transport formulations. Numerous studies have been made on hydrogen-air premixed flames under turbulent conditions in two and three-dimensional domains. Baum et al. [2] studied premixed $H_2/O_2/N_2$ flames in two-dimensional turbulence with detailed chemistry, and checked the validity of the flamelet assumption for premixed turbulent flames. Wang et al. studied swirling hydrogen-air premixed flames at different equivalence ratios [3] and investigated the effect of equivalence ratio on preferential diffusion effects and studied the role of small-scale eddies in interactions between turbulence and the flame front. A swirling hydrogen-air premixed flame at stoichiometric condition, with a moderate Reynolds number and a high swirl number, was studied by Wang et al. [4]

and the statistical properties and flame structures were examined. Baritaud et al. [5] compiled articles that dealt primarily with DNS of turbulent reacting flows. Echekki et al. [6] studied evolution of a premixed flame kernel in a turbulent flow field and proposed models for flame surface area and flame surface density (fsd). Results were compared with those from DNS of the evolution of a cylindrical flame kernel in two-dimensional turbulence. They found that the dominant contribution to the transport of fsd comes from turbulent strain and curvature. Vasudeo et al. [7] numerically investigated the flame kernel-vortex interactions using a detailed mechanism for hydrogen chemistry. A revised regime diagram for KV interactions was proposed with a broader range of KV interactions [7]. Studies have also been made on interactions between turbulence and chemistry in premixed flames. Hamlington et al. [8] studied interactions between turbulence and flames in premixed reacting flows in a three-dimensional unconfined domain and examined the effect of turbulence intensity on flame orientation and thickness of preheat and reaction zones. As more and more challenging and complicated problems with realistic conditions are numerically studied, there is a growing need for powerful post-processing packages that can help interpret, draw useful conclusions from and present the large amounts of data that result from such simulations. Zistl et al. [9] developed a library containing useful post-processing tools for analyzing and visualizing 2D and 3D flames and flow fields in turbulent reactive flows. This library was implemented in the MATLAB platform. Mansour et al. [10] studied flame kernel propagation in turbulent premixed methane flow experimentally, and found that the flame kernel structure starts with a spherical shape and changes to peanut-like structure and then to mushroom-like, and

eventually gets disturbed by turbulence. They also found that the average growth of the kernel in the first 100 μs is about three times faster than its development at later stages.

Thévenin et al. [11] compared DNS of turbulent methane flame kernels in two- and three-dimensions, with realistic chemistry. They developed a three-dimensional DNS code leading to reasonable computing times. They found that evolution of flame surface area, stretch rate, and flame front curvature show considerable differences between two- and three-dimensional computations. Kaminski et al. [12] studied flame growth and wrinkling in a turbulent flow using high-speed planar laser-induced fluorescence (PLIF) and 3-D large eddy simulations (LES). They observed that under low turbulence levels and at stoichiometric conditions, the flame kernel remained singly connected and nearly spherical in shape but with increase in turbulence or decrease in stoichiometry, formation of separated pockets was observed. Jenkins and Cant [13] studied curvature effects on flame kernels under various turbulence conditions. They studied the interactions of a premixed flame kernel with a field of isotropic turbulence. Different turbulence intensities were used to study the effects of turbulence on curvature of the flame kernel. They found that with an increase in the turbulence intensity, the alignment between the radius vector of the kernel and the surface normal vector decreases. Also, locations closer to the leading edge of the flame had curvature that was convex to the reactants, and locations closer to the trailing edge of the flame displayed moderately concave curvature. Dunstan and Jenkins [14] studied the effects of initial turbulent energy spectra on flame kernel development during initial stages of its growth, using DNS with single-step chemistry. Different integral length scales were used with two different turbulence intensities. They found the integrated reaction rates to reduce in

comparison to the equivalent laminar flame kernel, with decrease in length scales. This indicates the effects of enhanced turbulent heat transfer by Kolmogorov scale eddies.

Lange [15] investigated evolution of turbulent flame kernels using DNS on different clusters. A parallel code for DNS of reactive flows using detailed chemical kinetics and multicomponent molecular transport is presented. Performance of different clusters for problems of different sizes was studied. The said DNS code was used to study the evolution of flame kernel in $H_2/O_2/N_2$ mixtures, following induced ignition of the mixture. Gashi et al. [16] compared results from 2D OH PLIF and 3-D DNS for curvature and wrinkling of premixed flame kernels. They found a high level agreement between the results from these approaches, indicating that the simplified chemistry treatment employed in DNS may have a limited influence on freely propagating flames. They also find that the use of PLIF and DNS in combination is a powerful tool for flame analysis. Klein et al. [17] studied effects of turbulence on self-sustained combustion in premixed flame kernels using DNS. Different initial flame radii and turbulence conditions were used along with single step Arrhenius chemistry. It was found that for very small kernel radius, the heat transfer from the kernel overcomes the heat release due to combustion, leading to extinction of the flame kernel. This mechanism was found to be enhanced by turbulent transport. Turbulence intensity and length scales were found to adversely affect self-sustained combustion. Shalaby and Thévenin [18] used 3-D DNS with relatively high Reynolds number along with realistic chemistry for the study of propagation of an initially spherical, premixed methane flame kernel. DNS simulations were repeated several times to obtain statistically significant results, allowing for ensemble averaging of results. Chakraborty et al. [19] used 3-D DNS to study the effects of

mean flame curvature on reaction progress variable gradient and local turbulent strain rate of premixed kernels under decaying turbulence.

1.3 Statement of Objectives

The primary focus of this work is the study of initial and subsequent stages of a premixed flame kernel ignition of a stoichiometric hydrogen-air mixture under turbulent conditions using DNS. Different turbulence intensities and length-scales are used to obtain four different turbulent conditions. The results are compared with a reference case having laminar conditions. In the post-processing stage, Lagrangian derivatives of temperature and species ($\frac{DY_k}{Dt}$, $\frac{DT}{Dt}$), and production rates ($\dot{\omega}_k$) are used to study the initial stages of the kernel, and flame surface statistics and volumetric data are studied for the evolving kernel. The Lagrangian derivative corresponds to the terms on the transport equations that combine both the unsteady and the advective terms, leaving only diffusive transport and chemical sources terms on the right-hand side. These terms isolate the effects of the coupling of reaction and diffusion on the flame kernel structure and propagation.

1.4 Overview

This thesis is organized as follows,

- In Chapter 2, an introduction to the Pencil code is given; numerical scheme and boundary conditions used in the study are discussed. Cases considered for the study and details about post-processing of data are presented.
- In Chapter 3, results and discussions of the initial stages of the flame kernel are presented.

- In Chapter 4, results for the evolving kernel are presented and discussions are made.
- In Chapter 5, concluding remarks are presented and scope for future work is discussed.

CHAPTER 2

Numerical Implementation

In this chapter, the numerical implementation for the solution of flame kernels is discussed. First, the Pencil code, its governing equations and their numerical implementation are presented. Then, the specific implementation for the flame kernel solution is discussed.

2.1 The Pencil code

The Pencil code [1] is a public domain high-order finite difference code for DNS of weakly compressible turbulent reactive flows with or without particles and magnetic fields. This code was originally developed at the Turbulence Summer School of the Helmholtz Institute, Potsdam in 2001. It is the first open source DNS code with detailed chemistry available. The code uses explicit time-stepping to achieve good parallelization. It runs efficiently under message passing interface (MPI) on massively parallel shared- or distributed-memory computers. The code is highly modular and can be adapted for various problems. Typical applications of the code include simulations of magneto-hydrodynamic turbulence in a periodic box, convection in a slab with non-periodic upper and lower boundaries, self-gravity, non-local radiation transfer, dust particle evolution, turbulent combustion among others. Since the code solves equations along one-dimensional pencils in the *x*-direction, it is cache-efficient. This feature is advantageous in that auxiliary and derived variables consume very little additional memory. Even though the code is designed to be run

with MPI on supercomputers, it can be used on any computer running Unix or Linux with a Fortran 90 or 95 compiler without the MPI libraries. Users have the option of adding new physics and diagnostics to the code.

The code has several modules, which solve different parts of governing equations, advance the solution, handle diagnostics etc., in the 'src' directory. Each module has several subroutines. The 'samples' directory has some typical problems the code is used for. Each sample has a local 'makefile' and a 'cparam' file that determine the modules necessary and the processor layout for the particular sample problem, respectively. Further description of the code and its applications can be found in the Pencil code manual [20]. The governing equations, numerical schemes and boundary conditions used for the study are discussed in the following sections. A schematic diagram showing the basic structure of the code is given in Fig. 2.1.

The code uses a six-step mechanism [21] for hydrogen-air combustion reduced from Li et al. mechanism. The Li et al. mechanism [22] is a detailed 19-step reaction mechanism for hydrogen-air combustion.

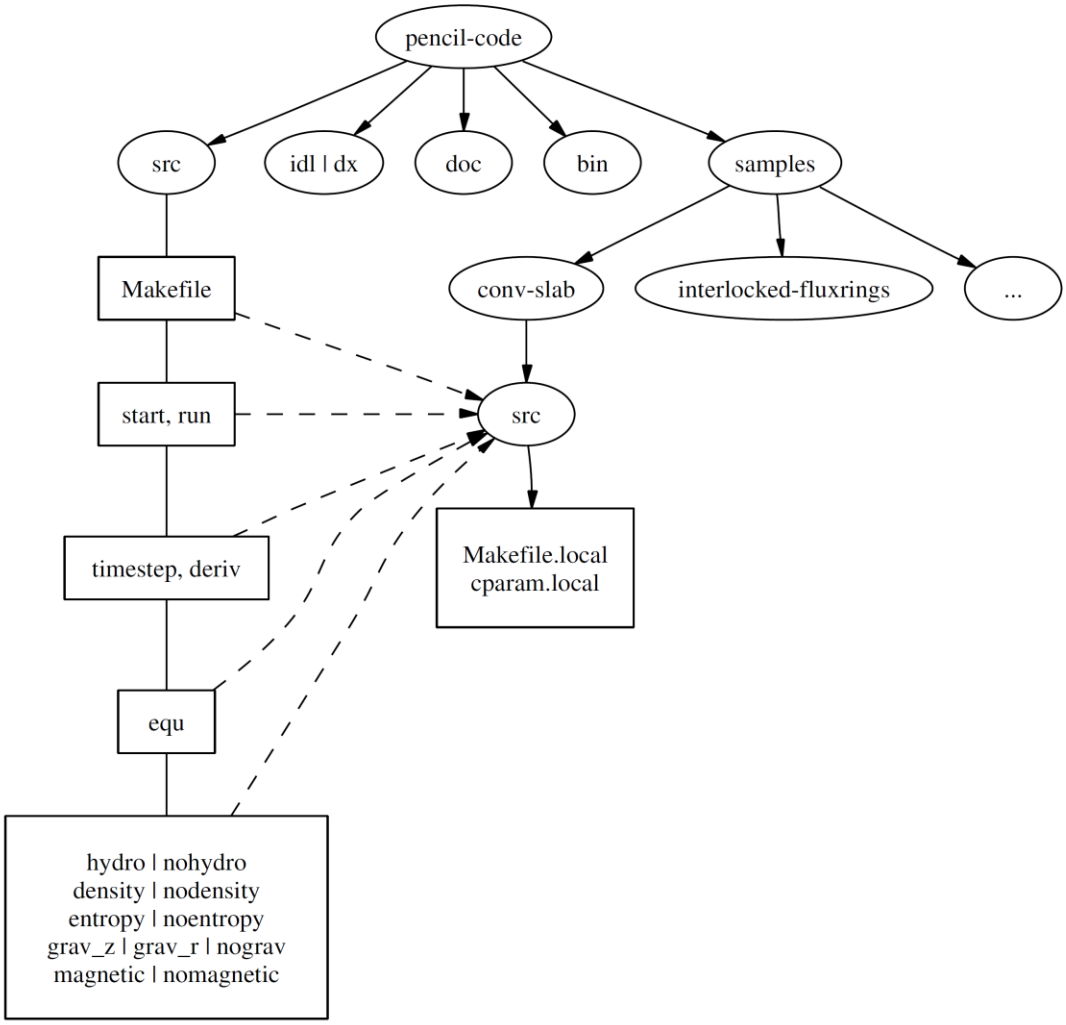

Figure 2.1: Directory tree of the Pencil code.

2.2 Governing Equations

In DNS, the complete system of Navier-Stokes equations is solved. The governing equations used by the code and for the study are given below [1],

- Continuity Equation

$$\frac{\partial ln(\rho)}{\partial t} + \boldsymbol{U}.\ \nabla \ln(\rho) = -\nabla.\boldsymbol{U} \tag{2-1}$$

- Momentum Equation

$$\frac{\partial \boldsymbol{U}}{\partial t} + \boldsymbol{U}.\nabla\boldsymbol{U} = \frac{1}{\rho}\left(-\nabla p + \nabla.(2\rho\vartheta\boldsymbol{S})\right) + f_b \tag{2-2}$$

- Energy Equation

$$(c_p - \frac{R}{m})(\frac{\partial ln(T)}{\partial t} + \boldsymbol{U}.\nabla \ln(T)) = \sum_k \frac{DY_k}{Dt}\left(\frac{R}{m_k} - \frac{h_k}{T}\right) - \frac{R}{m}\nabla.\boldsymbol{U} + 2\vartheta\boldsymbol{S}^2 - \frac{\nabla.\boldsymbol{q}}{\rho T} \tag{2-3}$$

- Species Transport

$$\frac{\rho DY_k}{Dt} = -\nabla.J_k + \dot{\omega}_k \tag{2-4}$$

The term DY_k/Dt is an illustration of a Lagrangian derivative in the transport equation for species *k*.

- Ideal Gas Equation

$$p = \frac{\rho RT}{m} \tag{2-5}$$

where $\frac{D}{Dt} = \frac{\partial}{\partial t} + \boldsymbol{U}.\nabla$ is the advective derivative, ρ is the density, $\boldsymbol{U}$ is the velocity vector, p is pressure, f_b is a volume force, $S_{ij} = \frac{1}{2}\left(\frac{\partial U_i}{\partial x_j} + \frac{\partial U_j}{\partial x_i}\right) - \frac{1}{3}\delta_{ij}$ is the trace-less strain tensor, c_p is the specific heat of the gas at constant pressure, R is the universal gas constant, h is the enthalpy, m is the molecular mass, ϑ is kinematic viscosity, T is the temperature, $\boldsymbol{q}$ is the heat flux, Y_k is the mass fraction of species k, J_k is the diffusive flux of species k and $\dot{\omega}_K$ is the production rate of species k.

For this study, detailed multi-component diffusion transport and variable thermal transport is used. So, mixture averaged quantities are used in calculations. Equations used to calculate some of the terms in the governing equations given above, are as follows,

- The viscosity, ϑ of the mixture is calculated using [1],

$$\vartheta = \sum_{k=1}^{N_s} \frac{X_k \vartheta_k}{\sum_{j=1}^{N_s} X_j \emptyset_{kj}} \tag{2-6}$$

where N_s is the number of species, ϑ_k is the single component viscosity, $X_k = \frac{Y_k m}{m_k}$ is the mole fraction of species k, and

$$\emptyset_{kj} = \frac{1}{\sqrt{8}}\left(1 + \frac{m_k}{m_j}\right)^{-\frac{1}{2}} \left\{1 + \left(\frac{\vartheta_k}{\vartheta_j}\right)^{\frac{1}{2}} \left(\frac{m_j}{m_k}\right)^{\frac{1}{4}}\right\}^2 \tag{2-7}$$

- The production rate of species k is given by [1],

$$\dot{\omega}_k = m_k \sum_{s=1}^{N_r} (\vartheta''_{ks} - \vartheta'_{ks})\{ \left(\frac{\rho_k}{m_k}\right)^{\sum_{\iota=1}^{N_s}(\vartheta'_{k\iota})} k_s^+ \prod_{J=1}^{N_s} X_J^{\vartheta'_{Js}} - \left(\frac{\rho_k}{m_k}\right)^{\sum_{\iota=1}^{N_s}(\vartheta''_{k\iota})} k_s^- \prod_{j=1}^{N_s} X_j^{\vartheta''_{js}}\} \tag{2-8}$$

where N_r is the number of reactions, m_k is the molecular mass of species k, $n_k = \frac{\rho_k}{m_k}$ is the

molar concentration of species k, ϑ'_{ki} and ϑ''_{ks} are the stoichiometric coefficients of species 'k' of reaction 's' on the reactant and product sides, respectively. The rate of reaction 's' is calculated using the Arrhenius expression [1],

$$k_s = B_n T^{\alpha_n} \exp(-\frac{E_{an}}{RT}) \tag{2-9}$$

where B_n is the pre-exponential factor, α_n is the temperature exponent, and E_{an} is the activation energy. All these coefficients are empirical and depend on the reaction mechanism.

- The species diffusion flux, $J_k = \rho Y_k V_k$. Where, V_k is the mixture averaged diffusion velocity and is given by [1],

$$V_k = -\frac{D_k d_k}{X_k} \tag{2-10}$$

$$d_k = \nabla X_k + (X_k - Y_k)\ \frac{1}{p}\ \nabla p \tag{2-11}$$

where D_k is the diffusion coefficient of species k.

- The heat flux, $\boldsymbol{q}$ is given by [1],

$$\boldsymbol{q} = \sum_k h_k J_k - \lambda \nabla T \tag{2-12}$$

where λ is the thermal conductivity of the mixture. Individual species conductivities are calculated taking into consideration the transitional, rotational and vibrational contributions.

- Enthalpy, h_i of the ideal gas mixture is calculated using [1],

$$h_i = h_i^0 + \int_{T_0}^{T} c_{p,i} dT \tag{2-13}$$

where h_i^0 is the enthalpy of formation of species i at temperature T_0 and $c_{p,i}$ is the specific heat at constant pressure, of species i.

The Pencil code evaluates all the terms on the right hand side of the evaluation equations along a one-dimensional ‘pencil’ and then goes on to evaluate the next pencil and so on. This implies that the derived quantities exist along pencils at any given point of time [1].

2.3 Numerical Schemes

The Pencil code uses sixth-order centered finite differences for spatial discretization and third- and fifth-order Runge-Kutta schemes for time advancement.

2.3.1 Spatial Discretization

High-order finite-difference schemes are an alternative to the use of spectral methods in the study of compressible turbulence. They are easier to calculate and can achieve the same level of accuracy as spectral methods [1]. For an equidistant grid similar to the one shown in Fig. 2.2, the equations for first and second derivatives using the sixth-order scheme are given below [1],

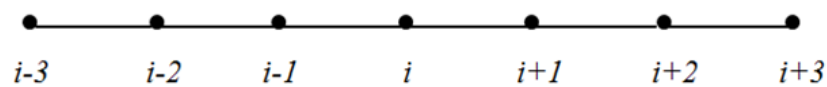

Figure 2.2: An equidistant grid.

- First derivative

$$f_i' = \frac{-f_{i-3}+9f_{i-2}-45f_{i-1}+45f_{i+1}-9f_{i+2}+f_{i+3}}{60\delta x} \tag{2-14}$$

- Second derivative

$$f_i'' = \frac{-f_{i-3}+9f_{i-2}-45f_{i-1}+45f_{i+1}-9f_{i+2}+f_{i+3}}{180\delta x^2} \tag{2-15}$$

where f_j is the value of function, f at node j and δx is the grid spacing.

2.3.2 Time Advancement

The code normally uses third-order Runge-Kutta time-stepping (RK3-2N) scheme for turbulence calculations. The RK3-2N scheme was developed by Williamson in 1980 [23]. It uses two chunks of memory, hence the name. The time-step is given as,

$$\delta t = \min\left(C_{\delta t}\frac{\delta x_{min}}{U_{max}}, C_{\delta t,v}\frac{\delta x_{min}^2}{D_{max}}, C_{\delta t,s}\frac{1}{H_{max}}\right) \tag{2-16}$$

where

$$\delta x_{min} = \min(\delta x, \delta y, \delta z) \tag{2-17}$$

and

$$U_{max} = \max(|u| + \sqrt{c_s^2 + v_A^2}\,) \tag{2-18}$$

where c_s is the speed of sound and v_A is the Alfven speed.

$$D_{max} = \max(\vartheta, \gamma\chi, \eta, D) \tag{2-19}$$

where $\chi = \frac{\lambda}{\rho c_p}$ is the thermal diffusivity and η is the magnetic diffusivity.

$$H_{max} = \max\left(\frac{2\vartheta^2 + \varsigma_{shock}(\nabla.u)^2 + \cdots}{c_v T}\right) \tag{2-20}$$

Here c_v is the specific heat at constant volume, ς_{shock} is bulk viscosity due to shock, and the dots indicate the presence of other terms in the energy equation (2-3).

The code has the option to use the fifth order Runge-Kutta-Fehlberg scheme with automatic adaptive time-step selection, based on the hydrodynamic constraints given above [1]. There

is also an option to use a constant time-step, *dt* instead of δt given above. This may be advantageous in many cases since it brings down the computational time. However, proper care has to be exercised while choosing *dt*, because if *dt* exceeds the viscous time step, the code may blow up or result in spurious data.

2.4 Initial and Boundary Conditions

2.4.1 Initial Conditions

For all the test cases in this study, the domain initially contained a homogenous mixture of hydrogen and air under stoichiometric conditions, the mass fractions being, Y_{H2}=0.024, Y_{O2}=0.230 and Y_{N2}=0.746. Ignition was achieved with the aid of an initial three-dimensional Gaussian temperature profile. The temperature profile is given below,

$$T(x,y,z) = T_0 + (T_1 - T_0)\exp\left(-\frac{r(x,y,z)^2}{r_{sp}^2}\right) \tag{2-21}$$

where T_o is the initial temperature, T_1 is the peak temperature and r_{sp} is the spread radius. The radius measuring the distance from the ignition source is expressed as follows:

$$r(x,y,z) = \sqrt{(x-x_o)^2 + (y-y_o)^2 + (z-z_o)^2} \tag{2-22}$$

where $(x_o,\ y_o,\ z_o)$ are the coordinates of the origin of the domain. An initial temperature, T_0 of 750 K and a peak temperature, T_1 of 1400 K was chosen for the study. A one-dimensional representation of the profile is shown in Fig. 2.3.

The reasons for choosing a preheated mixture (T_0 > 300 K) are explained below.

1. Due to the initial expansion of the gas before the onset of ignition and heat release, there is cooling of the gas in the domain.

2. In this study, an initial temperature profile is used instead of a flame kernel. Therefore, having hotter surroundings expedites the process of ignition and thus, brings down the time elapsed before heat release is observed. This is advantageous because the time that precedes ignition is additional cost to the computational time.
3. In practical combustion systems, ignition is preceded by a compression process that results in higher temperature and pressure from the intake air.

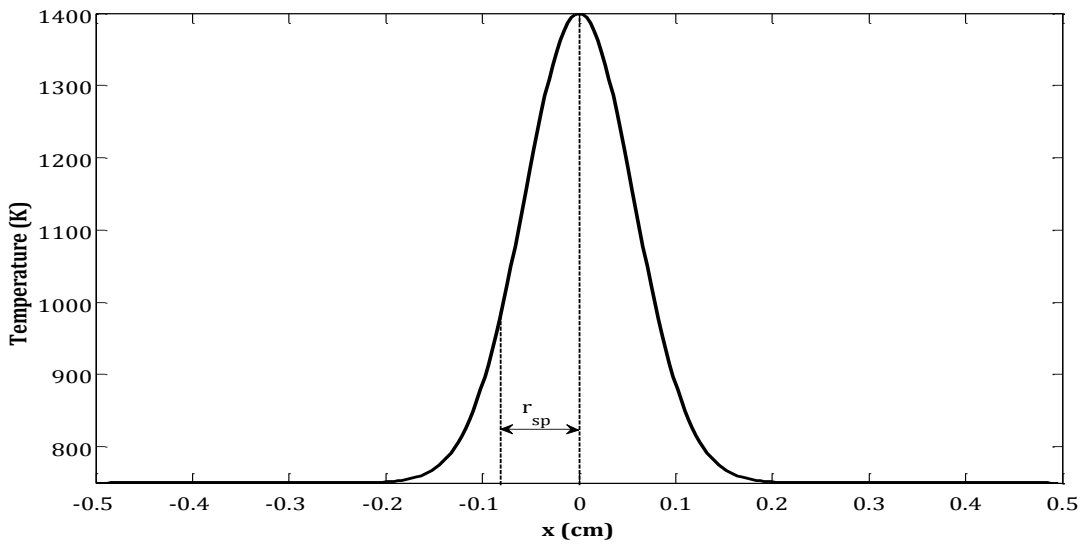

Figure 2.3: 1D representation of the temperature profile.

To avoid instabilities and shock waves at the boundaries, a hyperbolic tangent spatial filter was used for the velocity field during initialization. The filter is given as follows,

$$f_{\mathrm{u}} = \frac{1}{2}\left(\tanh\left(\frac{\delta_1 - r(x,y,z)}{\delta_2}\right) - \tanh\left(\frac{\delta_3 - r(x,y,z)}{\delta_2}\right)\right) \tag{2-23}$$

where δ_1= 0.405 cm, δ_3= -0.405 cm and δ_2= 0.002 cm. The filter takes the values of one between δ_1 and δ_2 and zero everywhere else.

2.4.2 Boundary Conditions

To avoid acoustic instabilities at the boundaries, the code uses non-reflecting Navier-Stokes Characteristic Boundary Conditions (NSCBC) [1]. NSCBC was first developed by Poinsot and Lele [24] as an extension to the Navier-Stokes equations. They developed an approach to account for viscous terms under the locally one-dimensional inviscid (LODI) assumptions, which came to be known by the name of NSCBC. Due to their robust nature, NSCBCs are quite suitable for direct simulations of turbulent reactive flows. In the current study, for isotropic turbulence generation in the domain prior to the application of the temperature profile, periodic boundary conditions are used for all directions. Once the profile is in place, non-reflecting outflow condition is used in all directions, allowing for the expansion of the gas. The Pencil code uses ghost zones to apply boundary conditions on physical and processor boundaries [20].

2.5 Cases Considered

For this study, ignition in a homogenous mixture of Hydrogen and Air under stoichiometric condition is studied at different combinations of turbulence intensities and length scales to give four different turbulence conditions. They are tabulated in Table 2.1.

Table 2.1: Turbulence conditions used for the study.

U_{rms}/S_L	0.2	0.8	0.2	0.8
L_T (mm)	1.6		4.2	

Results from these runs are compared with a reference case with laminar conditions, i.e., no mean flow or turbulence. Different length scales were obtained by changing the turbulence wavenumber, k_T. Wavenumber is related to the characteristic length scale by the relation,

$$k_T = \frac{2\pi}{L_T} \tag{2-24}$$

Wavenumbers of 1.5 and 4 were chosen for the runs. Turbulence intensities, U_{rms} of 2 m/s and 8m/s were used. The laminar flame speed, S_L of a hydrogen/air flame for an initial temperature of 750 K is 10 m/s [1].

For all the five cases, a cubical domain of 1cm^3 was chosen. Each direction was divided into 256 grid points. Eight processors were used for the *y*- and *z*-directions ($P_y = P_z = 8$) and one processor was used in the *x*-direction ($P_x = 1$). This resulted in a total number of 64 processors ($N_P = P_x \times P_y \times P_z$). The domain and processor layout are shown in Figs. 2.4 and 2.5.

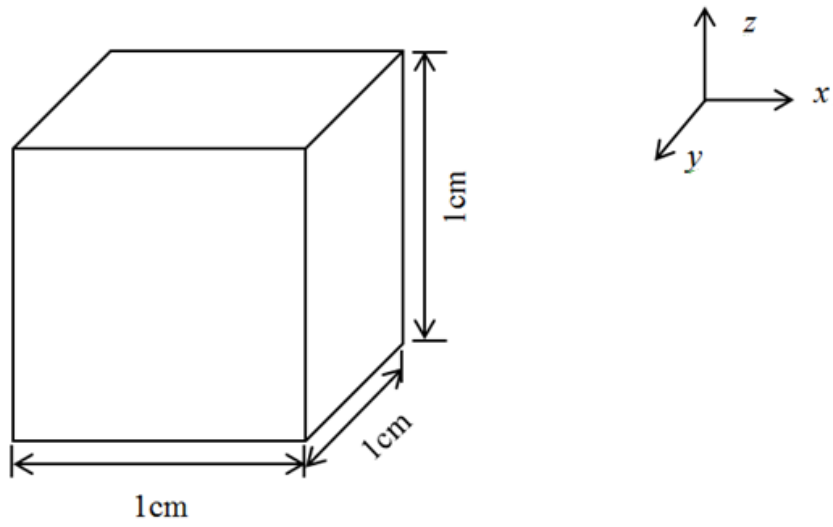

Figure 2.4: Simulation Domain.

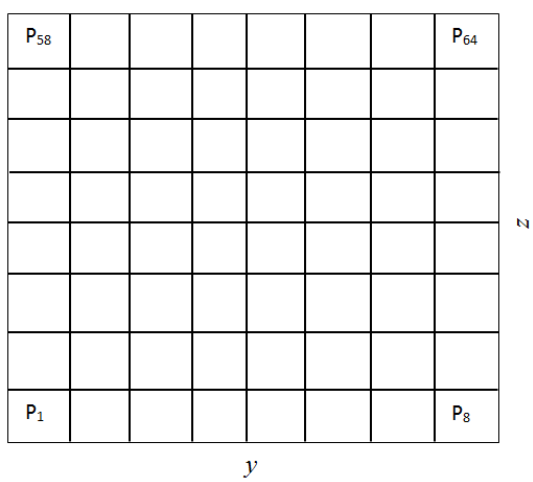

Figure 2.5: Processor Layout.

2.6 Post-processing

This study is divided into two main parts, 1) the investigation of initial kernel stages and 2) the study of evolving stages of the kernel. Different variables are used for the post-processing of these parts, details of which are given below:

1) For the study of initial stages of the kernel, evolution of Lagrangian derivatives of species ($\frac{DY_k}{Dt}$), flame surface area, and 2D contours of Lagrangian derivatives and reaction rates of intermediates, and species mass fractions (Y_k) are observed at stages close to the ignition of the mixture. As stated earlier, Lagrangian derivatives identify the role of the reaction-diffusion coupling on the structure and dynamics of the nascent flame kernel.
2) For evolving stages of the kernel, volume-averaged values of Lagrangian quantities ($\frac{D}{Dt}$), species production rates ($\dot{\omega}_k$), mass fractions (Y_k) are used. Effective flame radius (r_{eff}) and flame surface statistics, including probability density functions (pdf) of curvatures and strain rates are also studied.

CHAPTER 3

Studies of Early Kernel Stages

As stated earlier, the present study focuses on two stages of the premixed flame kernel evolution. The first stage corresponds to the onset of ignition and the early kernel evolution. Principal observations to be made concern whether turbulence conditions play any role in ignition delay; such an investigation is important because the classical view of kernel evolution states that ignition kernels tend to be too small to be affected by turbulence scales. For the study of early kernel stages, results from times close to the onset of ignition and heat release are used. The run conditions for the test cases are shown in Table 3.1,

Table 3.1: Run Conditions.

Domain Size (x x y x z)	1 cm x 1 cm x 1 cm
Grid Size (N_x x N_y x N_z)	256 x 256 x 256
Processors	64
Time-step, dt, (s)	0.75×10^{-8}
Initial temperature, T_0 (K)	750
Peak temperature of the Gaussian profile, T_1 (K)	1400
Fuel	H_2
Oxidizer	Air (O_2+3.76N_2)

3.1 Effects of turbulence on early kernels

In this section, the effects of different turbulence conditions on pre-ignition and ignition stages of the kernel are studied. Results are studied between the time at which the temperature profile is applied (t = 0) and a certain time after ignition is achieved (the first 60 - 80 μs).

3.1.1 Ignition Delay

Ignition is assumed to occur when heat release, and a proportional rise in temperature is observed. The time elapsed before heat release is observed is then a measure of the ignition delay. The effects of turbulence conditions on ignition delay are studied by observing the evolution of temperature of the domain with time. A plot of the maximum temperature in the domain at the early stages of the kernel is given in Fig. 3.1.

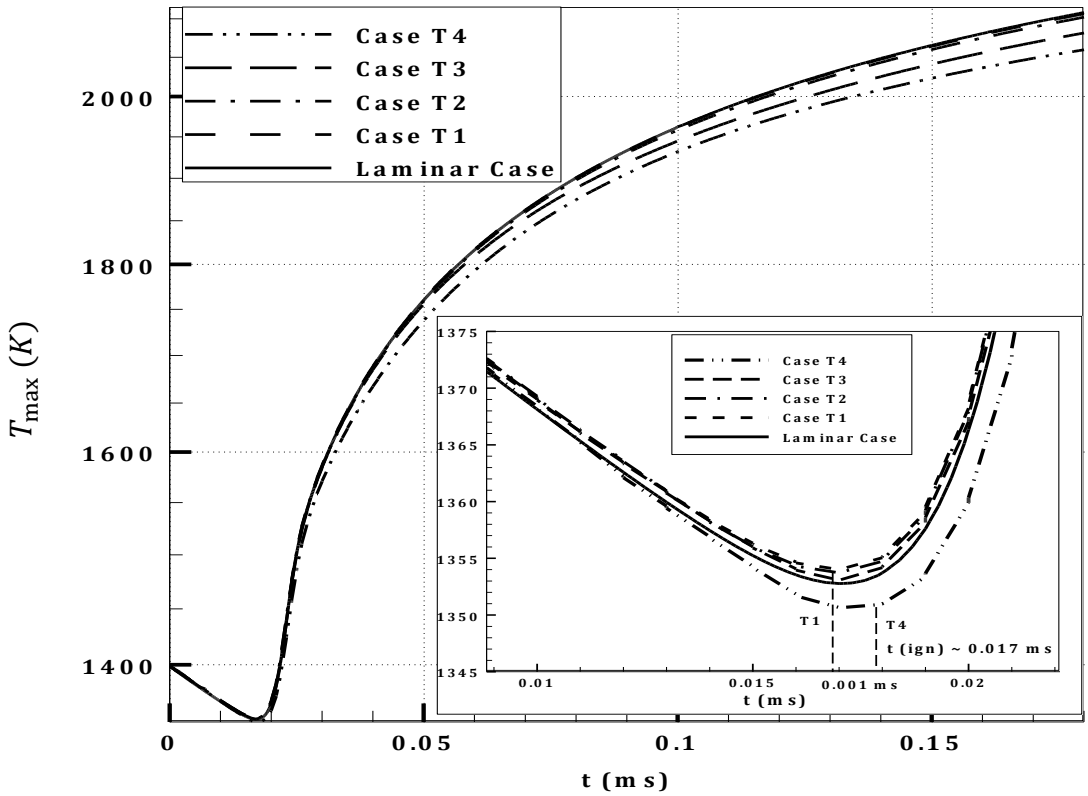

Figure 3.1: Maximum temperature in the domain plotted against time.

Here, T1, T2, T3 and T4 stand for cases with (U_{rms}/S_L, L_T) values of (0.2, 4.2), (0.2, 1.6), (0.8, 4.2) and (0.8, 1.6), respectively, where L_T is in mm. From Fig. 3.1, it can be seen that the maximum temperature initially decreases and then starts to increase once ignition is achieved, which in turn leads to rapid heat release. The initial decrease in T_{max} may be attributed to the initial expansion of the gas, before ignition starts, as discussed in Chapter 2. The expansion of the gas at the center of the domain is due to the diffusion of intermediates out of the kernel. A 1D representation of this temperature drop is shown in Fig. 3.2. To support this claim, velocity vectors (v and w components) for different cases are shown in

Fig. 3.3, against a contour of ln(T), at t = 0.017 ms. The viewing window is 0.15 cm^2 (-0.075 cm to 0.075 cm) in the y - z plane at x = 0 cm. From the figures, it can be observed that the velocity vectors are pointing away from the kernel center. This trend is very clear for the laminar case. Since the contours show y – z planes, the u component of the velocity field has not been shown. This signifies diffusion of species away from the hot kernel center. Because of the presence of a high temperature peak, intermediates start to form immediately after the Gaussian temperature profile is imposed. The production of intermediates is expedited in the presence of a preheated mixture [25]. A certain amount of intermediates need to be formed before ignition is achieved [25]. Since a preheated mixture is used in the current study, the process of ignition is assumed to be expedited. The peak temperature required to ignite the mixture in the case of an initial spherical Gaussian temperature profile decreases rapidly with the spread radius of the Gaussian profile and the number of dimensions in the problem [25]. For a 3D Gaussian profile with r_{sp} of 0.08 cm, the ignition temperature is around 1200 K [25]. The fact that the peak temperature of the current Gaussian profile is 1400 K also possibly expedites the onset of ignition. It can be seen that ignition happens at around t = 0.017 ms. Upon close observation, it is clear that ignition occurs at almost the same time for T1, T2 and T3 and laminar cases. This is expected because ignition chemistry time scales are expected to be much faster than any transport scales associated with diffusion or the modulation of this diffusion by turbulent mixing. Nonetheless, some minor differences can be seen. On closer observation, it can be seen that ignition occurs first for case T1, followed by T2 and T3, the laminar case, then finally case T4. The difference in ignition delays for cases T1, T2, T3 and the laminar case is too small, and so, the mixture in these are assumed

to ignite at about the same time. The overall difference in delay between cases T1 and T4 is only about 1 μs, which is not too significant. However, we can make the following observations. Case T4 has relatively the highest ignition delay. This trend indicates that ignition delay is shorter for less-intense, larger-integral scale turbulence. The fact that ignition is preempted for cases T1-T3 prior to the laminar case reflects the complex interactions between turbulence and chemistry during ignition. Further insight into the effect of turbulence on ignition delay is gleaned by studying the contours of Lagrangian derivatives and reaction rates of HO_2, shown in Figs. 3.4 and 3.5, respectively, soon after ignition is observed. The viewing window is 0.3125 cm^2 in the y - z plane at x = 0 cm. The HO_2 is an important intermediate, since it gives an insight into the interaction between turbulence and chemistry at times close to ignition. From Fig. 3.4, it is clear that the Lagrangian derivative of HO_2 for T1 and laminar cases are almost similar, with differences between the contours becoming more pronounced as the differences in the parameters for a certain case and those for the laminar case become more prominent. Case T4 differs the most from the laminar case, as can be seen from the said figure. Since the Lagrangian derivative combines the effect of diffusion and reaction, contours of reaction rates of HO_2 are studied for two cases that differ the most from each other, case T4 and the laminar case. It is clear from Fig. 3.5 that for case T4, the contribution of diffusion to the Lagrangian derivative is more significant compared to the laminar case. This is because smaller-scaled turbulence tend to enhance diffusion of radicals away from the nascent kernel. This in turn may lead to delays in the onset of ignition, as observed for case T4 in Fig. 3.1. Based on these observations, it is found that smaller-scaled and more intense turbulence initially inhibits growth of the kernel to a small

extent, in comparison with the larger-scaled and less intense cases of turbulence and the laminar case. Thus, it is found that turbulence conditions may expedite or delay the process of ignition, but because of the lack of significant differences in the effects these cases have on ignition delay, it is difficult to generalize these observations for other turbulence conditions. Further insight into the difference between the two turbulence effects is gleaned from further observations below.

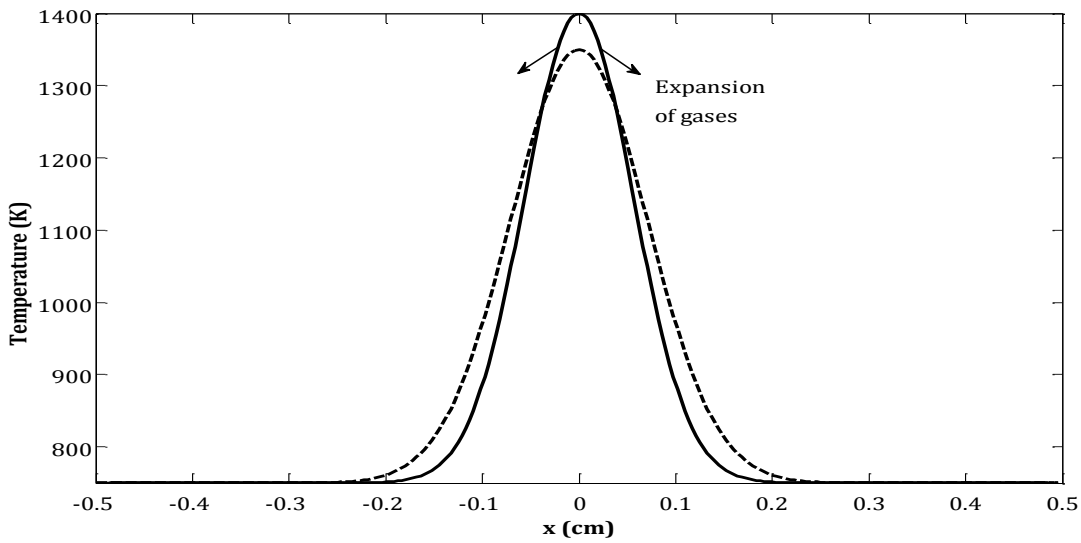

Figure 3.2: 1D representation of the temperature drop at the center of the domain, due to the expansion of gases.

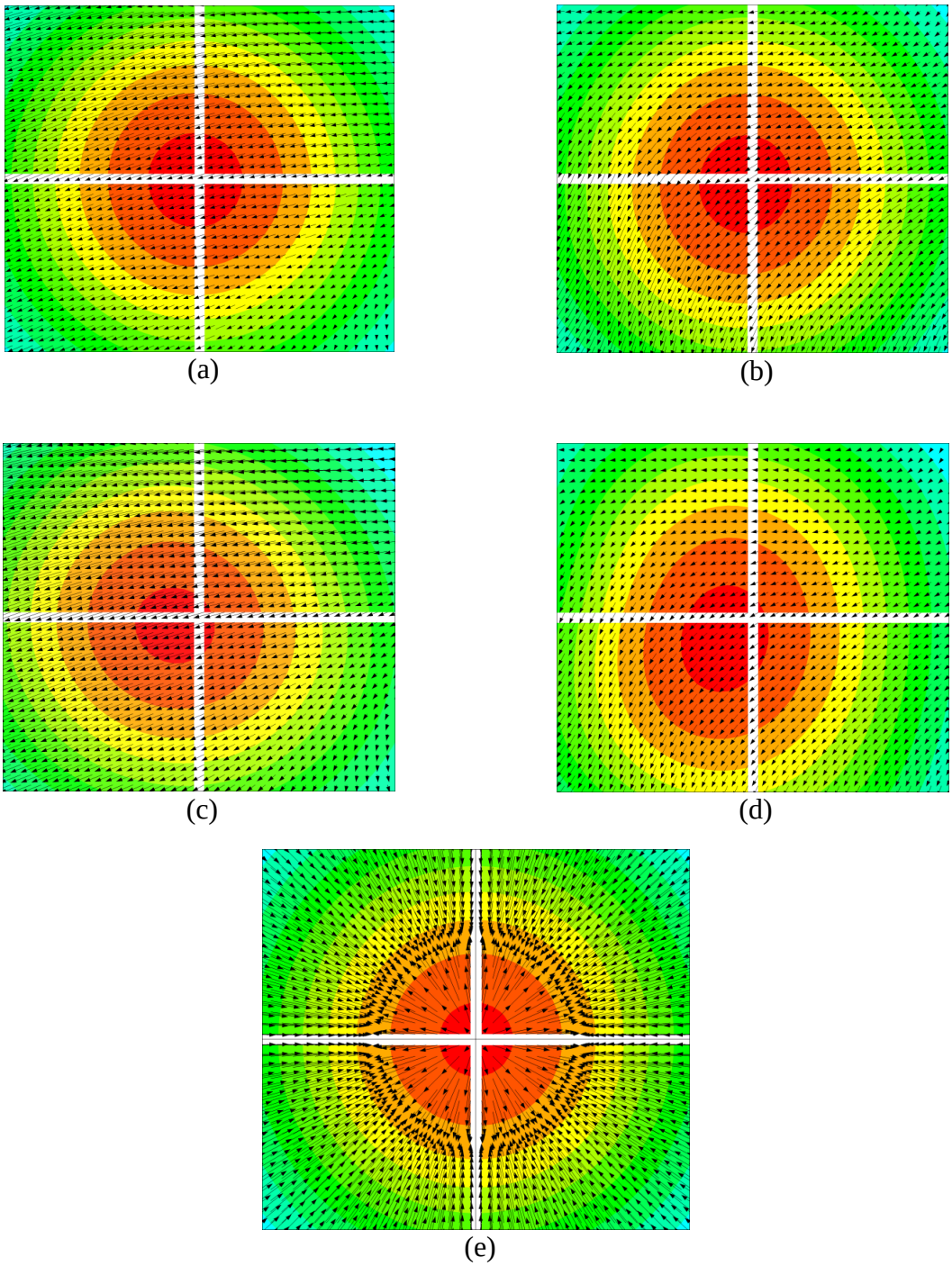

Figure 3.3: Velocity vectors (y –z plane) for (a) Case T1 (b) Case T2 (c) Case T3 (d) Case T4 and (e) Laminar Case, at t = 0.017 ms and x = 0 cm.

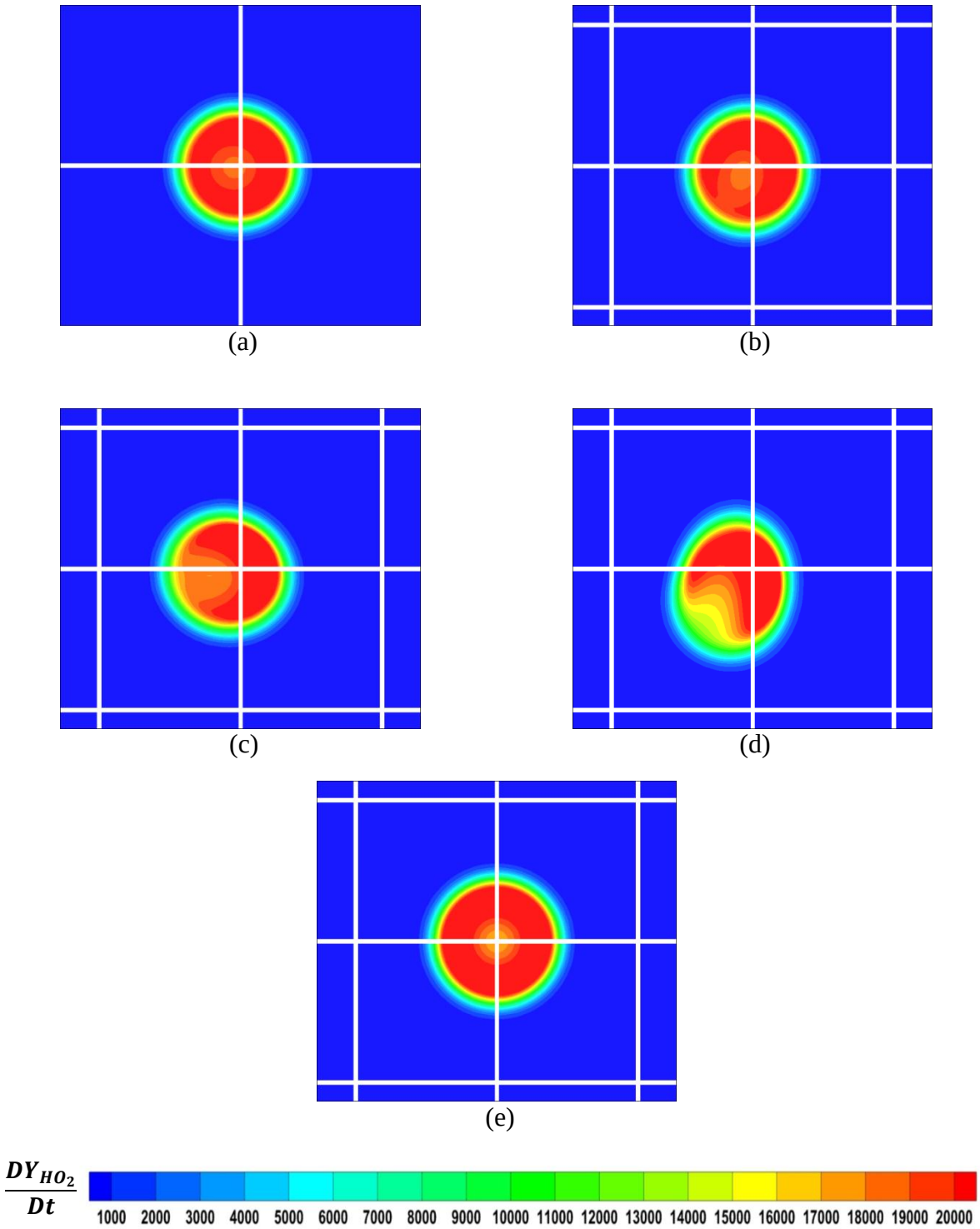

Figure 3.4: Lagrangian contours ($y - z$ plane) of HO_2 for (a) Case T1 (b) Case T2 (c) Case T3 (d) Case T4 and (e) Laminar Case, at t = 0.02 ms and x = 0 cm.

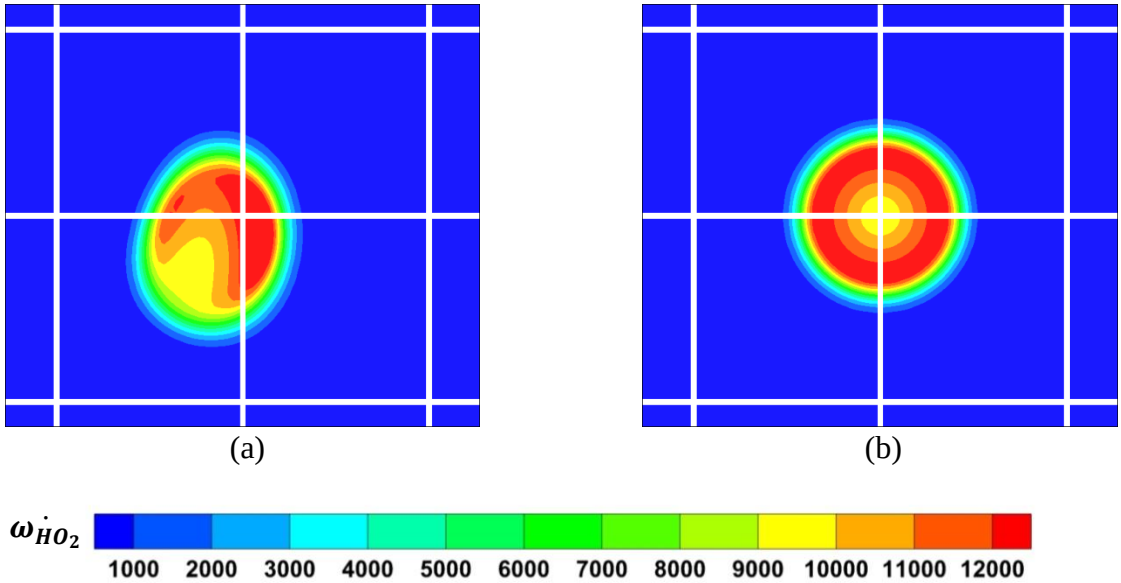

Figure 3.5: Reaction rate contours ($y - z$ plane) of HO_2 for (a) Case T4 and (b) Laminar Case, at t = 0.02 ms and x = 0 cm.

3.1.2 Reaction Progress and Kernel Shape

Reaction progress is studied by plotting the evolution of integrated reaction rates and Lagrangain time derivatives of H_2O and HO_2 during the initial stages of the kernel. As discussed earlier, the Lagrangian time derivative measures the balance between reaction and diffusion and does not include the effect of motion, except indirectly through its effects on scalar gradients and diffusion. The shape of the kernel is studied by using mass-fraction contours of HO_2 for the different cases soon after ignition, at t = 0.02 ms.

Figure 3.6 shows the evolution of logarithm of volume-integrated HO_2 reaction rate, during the initial stages of kernel evolution (first 100 μs from the time from the time when the temperature profile is applied). The inset shows evolution of non-logarithmic integrated reaction rate of HO_2 during the initial stages (first 60 μs). The difference between the

different cases is more clearly evident in the evolution of non-logarithmic$\langle \dot{\omega}_{HO_2} \rangle$, as can be seen from the inset. HO_2 is an important intermediate species for tracking the onset of ignition in hydrogen chemistry. The onset of its production indicates the initial stages of chemistry leading to the radical build-up characteristic of ignition, prior to the onset of rapid heat release.

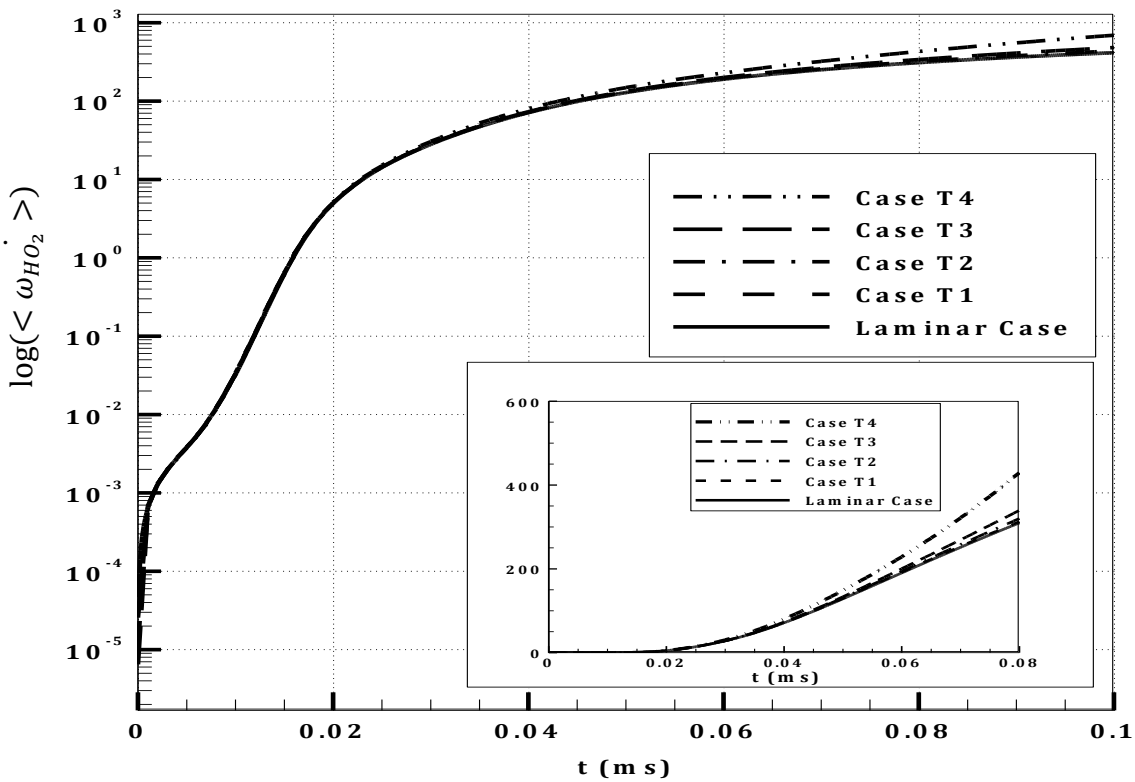

Figure 3.6: Reaction rate of HO_2 during the initial stages of the kernel.

It can be seen from Fig. 3.6 that effect of turbulence on the integrated reaction rate of HO_2 during the initial stages of the kernel cannot be clearly distinguished from the laminar

case, until about 0.06 ms. Beyond t = 0.06 ms, turbulence seems to enhance the production of HO_2. HO_2 is produced before the subsequent radical build-up of H, OH and O during intermediate stages of the ignition process. Thus, an increase in the production of HO_2 would mean an enhancement of reaction progress. It can be observed that the enhancement in reaction rate is highest for Case T4, followed by T3, T2, T1 and laminar cases. This may initially appear counter to the observation made above regarding ignition delay related to case T4 relative to the laminar case and cases T1, T2 and T3, but this shows that beyond a certain time after ignition, smaller scaled turbulence enhance the reaction progress. The other intermediates show trends that are closer to H_2O than to HO_2. Evolution of integrated reaction rate of H_2O with time during the early stages of the kernel is given in Fig. 3.7. The production rates for the different cases appear almost identical until the first 60 μs of kernel growth, but beyond t = 0.06 ms, turbulence enhances the production rate of H_2O. This enhancement is highest for case T4, followed by T3, T2, T1 and laminar cases, as can be seen in the inset of Fig. 3.7. This shows that smaller-scaled turbulence improves production of H_2O, thus enhancing the overall reaction progress. It is to be noted that HO_2 reaction rate is higher than that of H_2O initially. This is because of the fact that there is a temperature profile at t = 0. This serves as an ignition source and leads to the production of some intermediates (mainly HO_2 and H) immediately after the start of the run. Whereas, H_2O production takes some time to start.

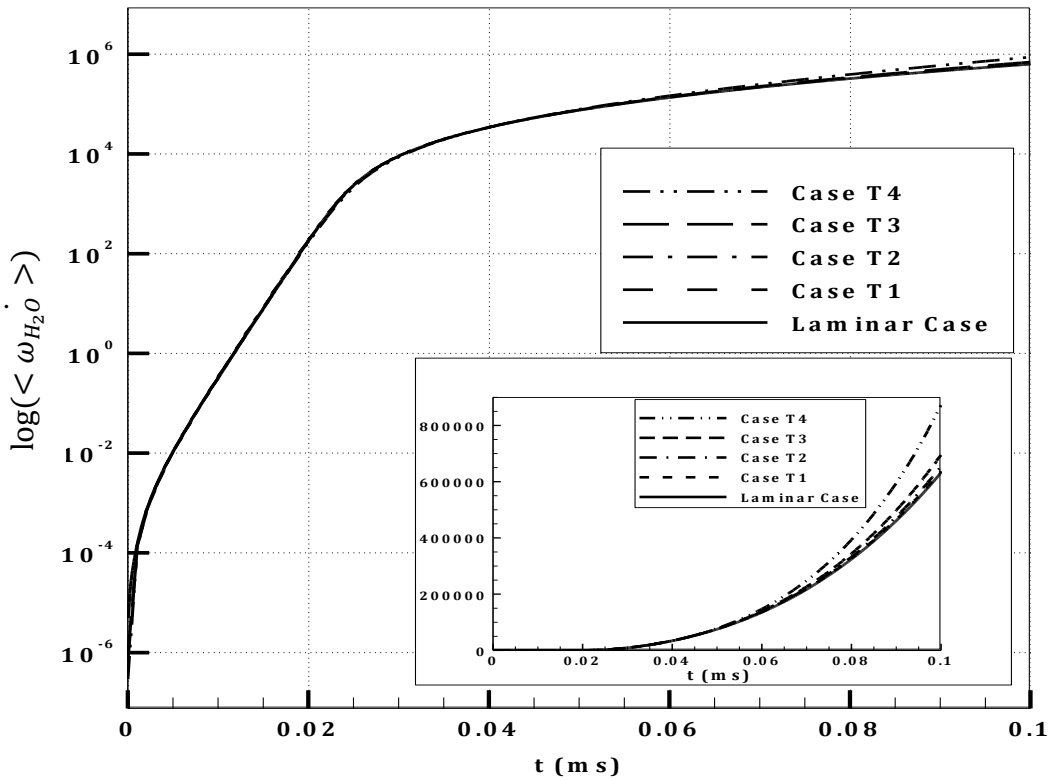

Figure 3.7: Reaction rate of H_2O during the initial stages of the kernel.

To understand what happens to the case of intense small scales (case T4), we look at the volume integral of the Lagrangian time derivative of both H_2O and HO_2. Integrated Lagrangian time derivative of H_2O is plotted against time for the early kernel stages in Fig. 3.8 (a). It is observed that differences in integrated Lagrangian derivative of H_2O for the different cases is not significant until about 0.06 ms. Beyond that point, smaller scales and higher intensity of turbulence seem to enhance $< \frac{DY_{H_2O}}{Dt} >$. This is due to the fact that beyond 0.06 ms, the contribution of the reaction rate is more significant to the Lagrangian time derivative of H_2O. Also, as shown earlier, the enhancement of reaction rate of H_2O is highest for case T4, followed by T3, T2, T1 and the laminar case. The temporal evolution of

integrated Lagrangian time derivative of HO_2 during the early kernel stages in Fig. 3.8 (b). As for H_2O, appreciable differences in the values of integrated Lagrangian time derivatives of HO_2 begin to appear only beyond a certain point of time after ignition, which as can be seen from the said figure, is close to 0.04 ms. The trend in enhancement is very similar to H_2O, with highest values observed for case T4, followed by cases T3, T2, T1 and the laminar case. Higher intensity small scale turbulence locally exerts straining effects on the nascent kernel that enhances the rate of diffusion of the species present during the initial stages of ignition (represented here through HO_2). Invariably, every mechanism that inhibits the formation of these initial radical species, will also delay the ignition process. This effect is expected to subside at later stages of the kernel evolution as turbulence will play a more wrinkling role and less of a straining role on the flame kernel. As time progresses, turbulence clearly enhances the Lagrangian time derivative values for both H_2O and HO_2.

Thus, it is clear that there are no appreciable differences in integrated quantities until the first 40-60 μs, but differences can be seen in instantaneous contours of these quantities, as was observed in Figs. 3.4 and 3.5. With these observations, it is clear that the effect of turbulence conditions on characteristics of the flame kernel, for cases that are close to the laminar case, is not significant during the early stages, but cases whose conditions differ significantly from the laminar case show appreciable differences in their effect on flame chemistry and growth.

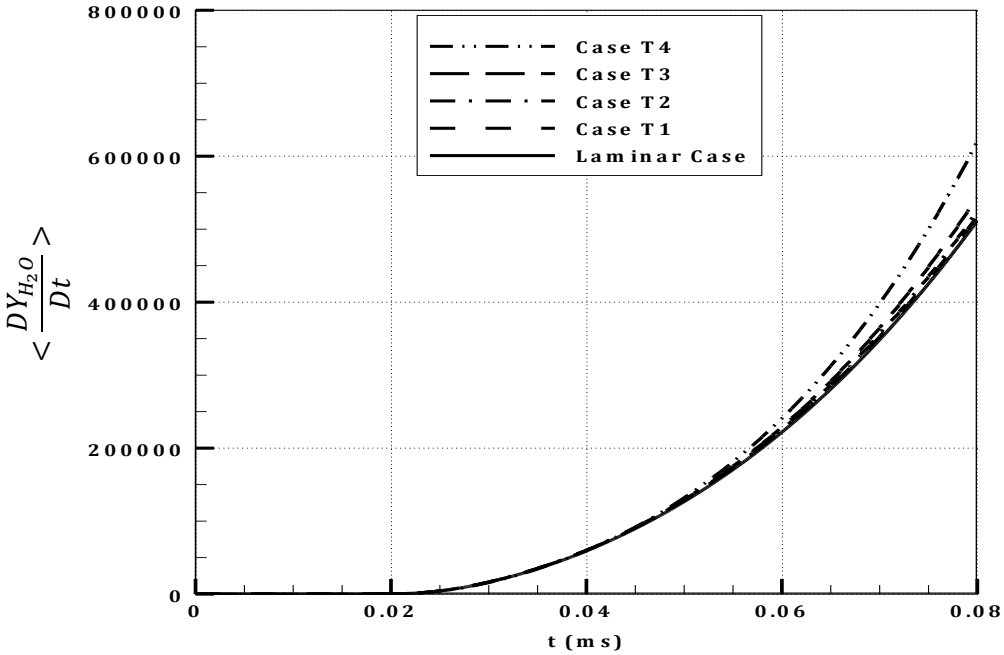

(a)

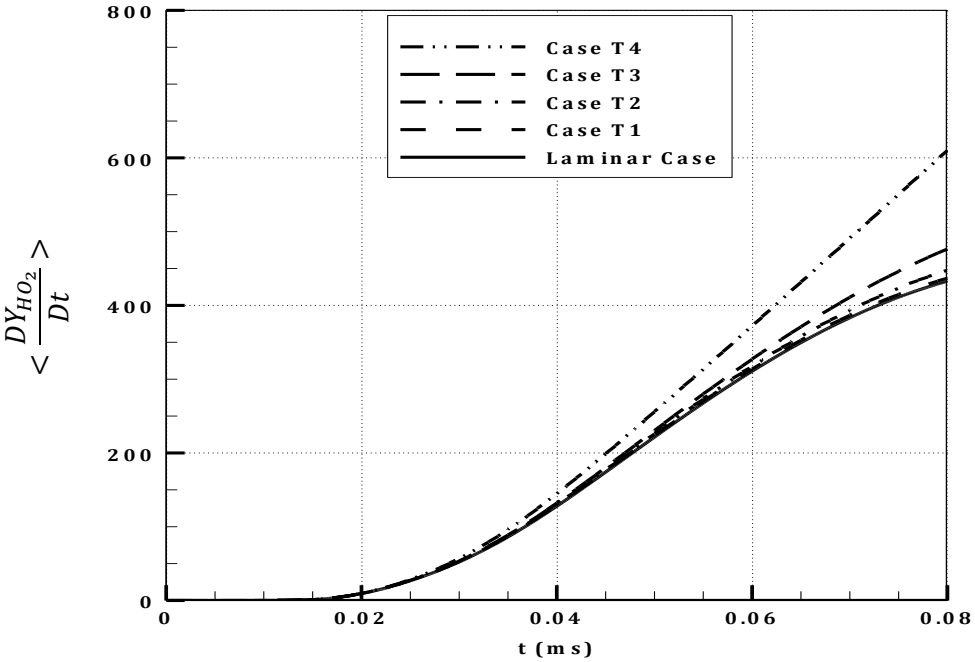

(b)

Figure 3.8: Initial Lagrangian evolution of (a) H_2O and (b) HO_2.

Mass fraction contours of HO_2 (magnified) for the different cases are given in Fig. 3.9. The figures are views of y - z planes at x = 0 cm. The viewing window is 0.5 cm^2 (-0.25 cm to 0.25 cm in y- and z- directions, at x = 0 cm). From the figures, it is clear that HO_2 mass fraction is higher at the reaction zone, and thus, it can be used as a marker for the reaction zone. These contours represent the state of the kernel at t = 0.02 ms after the temperature profile is imposed. Kernels in T1 and laminar cases are almost spherical but the kernel in case T1 is slightly off-center. Cases T2 and T3 show slight changes of shape and position of the kernels. The kernel in T4 has undergone the highest change in shape. Thus, smaller-scaled and more intense turbulence starts to affect the kernel structure very early in its growth resulting in significant straining of the nascent kernel and increased rates of diffusion of initial species of ignition (e.g. HO_2 and H_2O_2) out of the kernel, further delaying the radical build-up. As illustrated in the figure, larger scales simply serve to advect the kernel. This effect is more pronounced for the larger turbulence intensity cases, as can be observed by comparing cases T1 and T3. Also, the reaction zone for case T4 appears deformed and stretched due to the effect of straining by smaller-scaled and more intense turbulence.

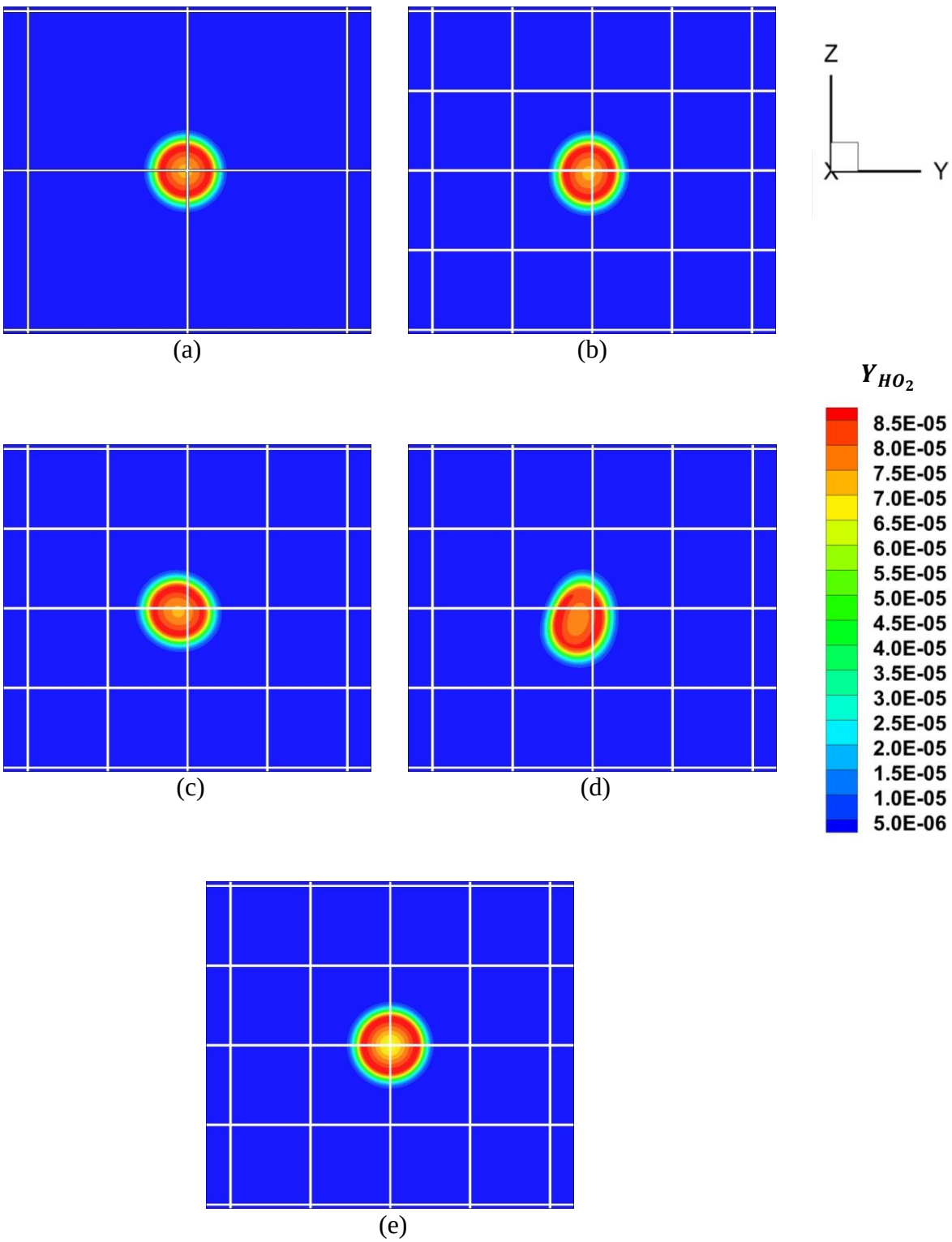

Figure 3.9: Mass fraction contours ($y - z$ plane) of HO_2 for (a) Case T1 (b) Case T2 (c) Case T3 (d) Case T4 and (e) Laminar Case, at t = 0.02 ms and x = 0 cm.

3.1.3 Flame Surface Area and Effective Radius

The flame surface area and effective radius of the kernel for the early stages are shown in Fig. 3.10. It is important to note that a definition of a kernel radius may not be meaningful until a premixed flame is established (after 0.04 ms or so). Prior to that, the surface area simply tracks a contour, which corresponds to a temperature equal to 1400 K. From the figure, it can be seen that the volume of ignition is larger for the laminar case (due to the straining of the turbulence conditions). Even so, once the kernel is established, turbulence tends to increase the flame area through wrinkling, as expected. The rapid growth of the surface area at early stages of kernel growth is associated with gas expansion away from the ignition point and flame propagation. The trend is similar for effective radius of the kernel. Effective radius is the radius a sphere would have if its surface area were equal to the area of the kernel. Details about the calculation of the effective radius are given in section 4.2 of the following chapter.

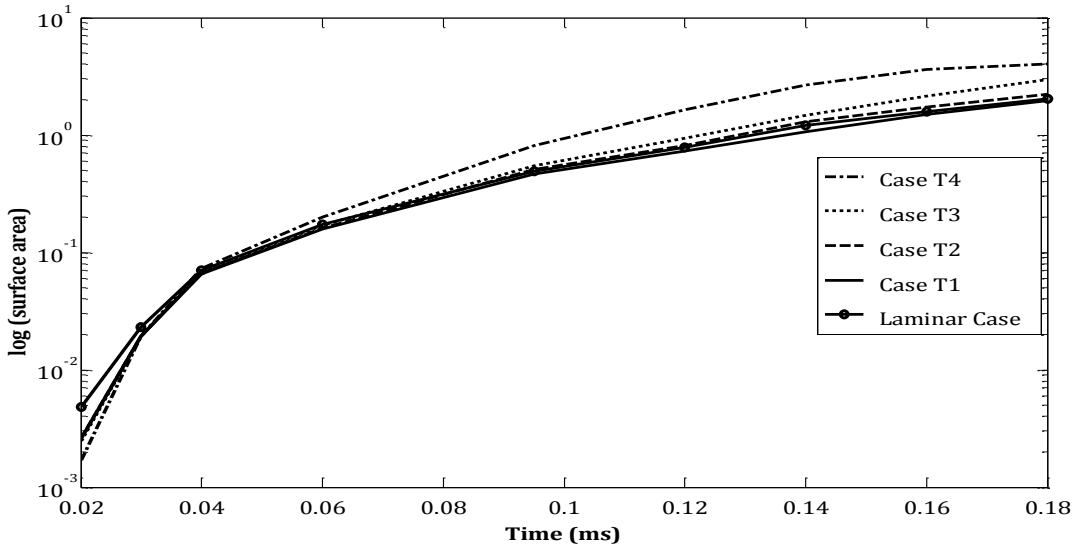

(a)

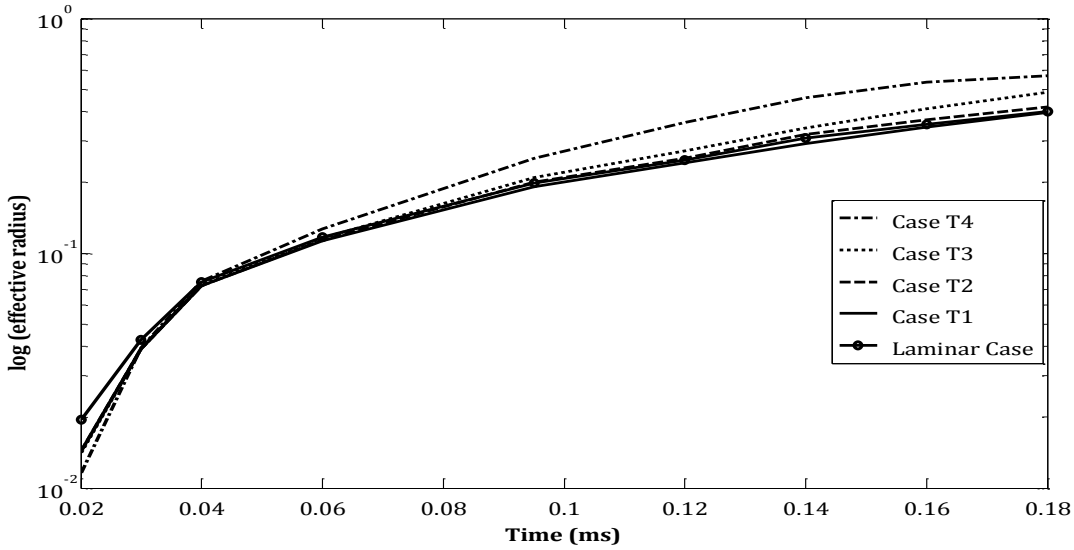

(b)

Figure 3.10: Logarithm of (a) Surface area and (b) Effective radius, against time.

3.2 Summary

It is thus observed that turbulence may or may not delay the process of ignition, depending on the turbulence conditions for the problem at hand. It is observed that smaller-scaled and more intense turbulence has slight delay in achieving ignition, in comparison with the laminar case. However, the difference in ignition delays for the cases considered is not significant enough to generalize this observation. Studying Lagrangian derivative and reaction rate contours of HO_2 at early stages suggest that smaller-scaled and more intense turbulence enhances diffusion, thus making its contribution to the Lagrangian time derivative significant in comparison with that of the reaction rate. On the other hand, for the laminar case, the contribution of reaction rate overshadows that of diffusion. Turbulence has no discernible effect on integrated reaction rates of HO_2 or H_2O during the first 40-60 μs of kernel development, but beyond that point, turbulence appears to enhance the integrated reaction rates of both HO_2 and H_2O. This enhancement is found to be higher for smaller-scaled and more intense turbulence. Thus, T4 has the highest observed enhancement, followed by T3, T2, T1 and laminar cases. The kernel shape is altered to the greatest extent during the early stages for case T4, at a time close to ignition. Also, the reaction zone appears deformed for case T4, suggesting that smaller scales and higher intensity of turbulence subject the kernel to straining and curvature effects very early in its growth, which may lead to extinction or shredding of the flame at later stages. The flame surface area and the effective radius of the flame kernel are relatively higher for the laminar case, followed by cases with larger-scaled and less intense turbulence, during the early stages.

CHAPTER 4

Flame Kernel Evolution

In the previous chapter, we discussed the early stages of the flame kernel evolution, and addressed primarily the process of ignition. In this chapter, we consider the subsequent stages of the flame kernel evolution. The results are presented in terms of volumetric data along with discussions of surface statistics of the flame kernel.

4.1 Volumetric Data

Contours and iso-surfaces of species mass fractions and mean temperature are used to study the shape and nature of the flame kernel. Integrated Lagrangian time derivative of species and reaction rate of species are used to investigate the effects of turbulence on chemistry and diffusion transport. A plot of the integrated (volume-averaged) Lagrangian time derivative of H_2O against time for different test cases is given in Fig. 4.1. T1, T2, T3 and T4 stand for cases with (U_{rms}/S_L, L_T) values of (0.2, 4.2), (0.2, 1.6), (0.8, 4.2) and (0.8, 1.6) respectively.

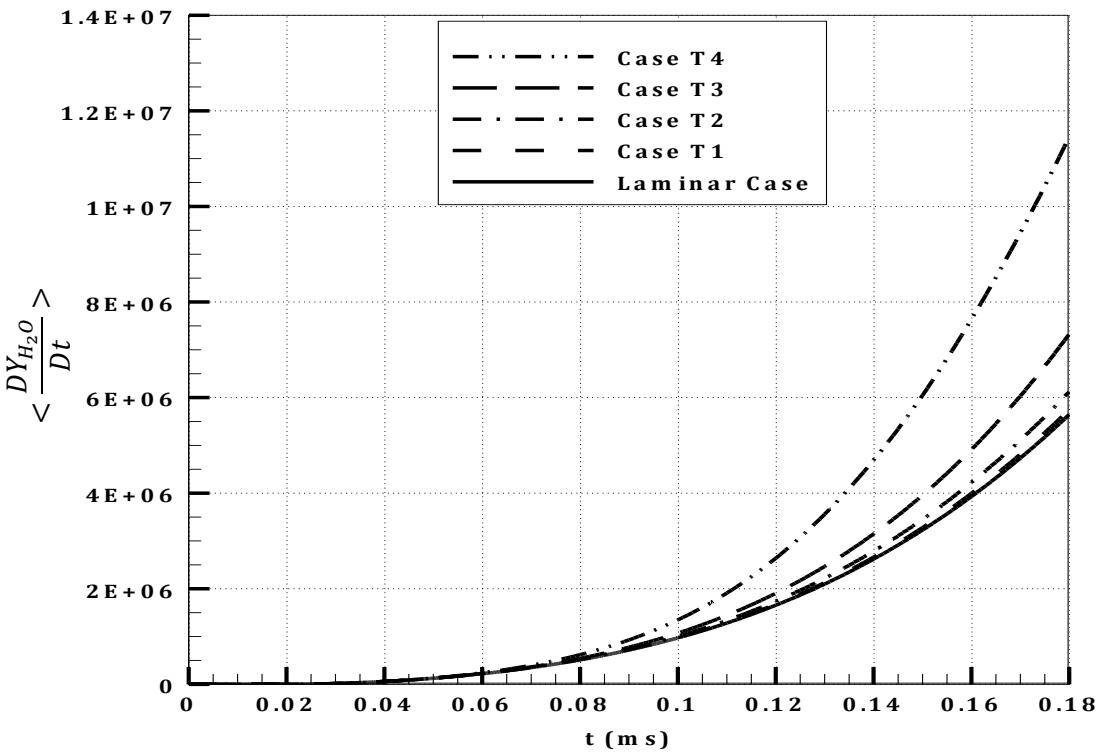

Figure 4.1: Variation of integrated Lagrangian time derivative of H_2O with time.

From Fig. 4.1, it is clear that turbulence enhances the reaction rate of H_2O. Upon further inspection, it is found that the enhancement increases with the decrease in turbulence length scale (L_T) at a given turbulence intensity (U_{rms}/S_L) and with the increase in turbulence intensity at a fixed value of turbulence length scale. The highest enhancement is observed for the case with the lowest length scale and the highest turbulence intensity, i.e. L_T = 1.6 and U_{rms}/S_L = 0.8. This trend is indicative of the importance of small-scale eddies in flame chemistry. These eddies tend to enhance the flame surface area and thus result in increased area of contact between the reactants, improving the overall reaction progress. Thus, for H_2O, the role of diffusion is not as significant as that of the reaction rate at subsequent stages of

kernel growth. This makes the values of the Lagrangian time derivatives higher for cases with smaller length scales and more intense turbulence.

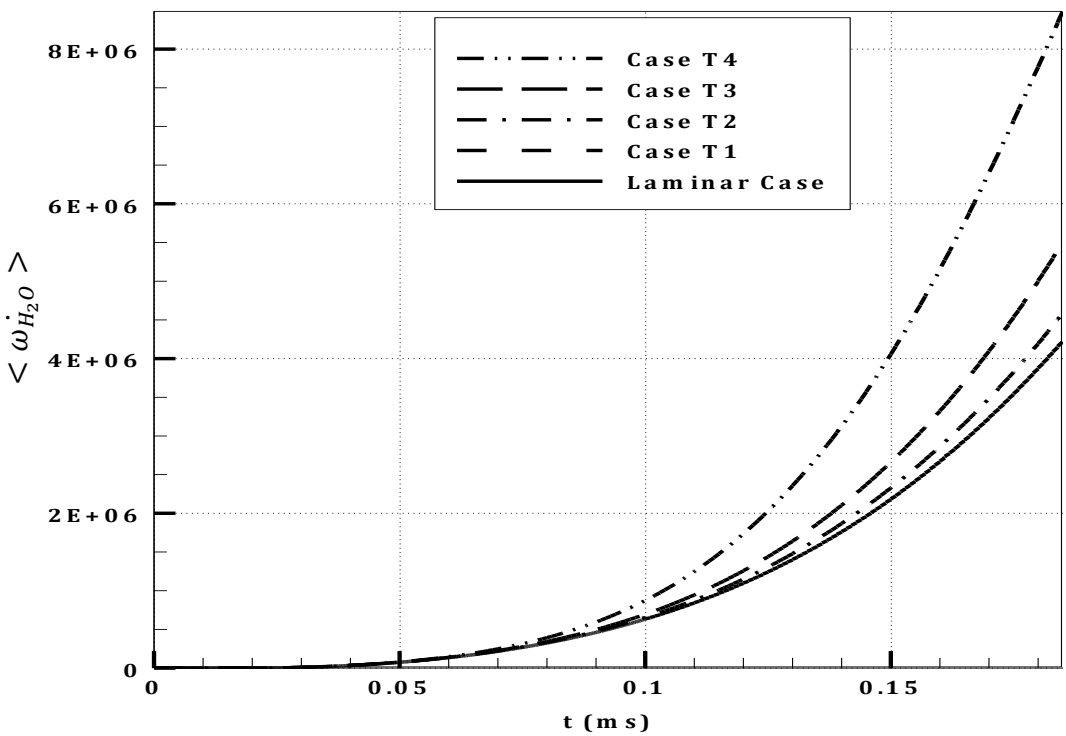

Figure 4.2: Integrated reaction rate of H_2O plotted as a function of time.

Integrated (volume-averaged) reaction rate ($\dot{\omega}_k$) of H_2O is plotted against time in Fig. 4.2. It is clear from Fig. 4.2 that turbulence enhances the production of H_2O. The enhancement is highest for case T4, followed by T3, T2, T1 and laminar cases. This enhancement is due to the same reasons stated above for the Lagrangian time derivative of H_2O. Similar trend is observed for the intermediates H, O and OH. Further insight into the effects of turbulence on diffusion and flame chemistry can be obtained by studying the

instantaneous contours of Lagrangian time derivative of HO_2 for the different cases, which are shown in Fig. 4.3.

From Fig. 4.3, it can be observed that the values of the Lagrangian time derivative are higher at the flame surface. This is due to the higher values of reaction rate at the reaction zone, which is at the flame surface. For case T4, islands of higher reaction rates are observed both inside and outside the flame surface, as can be seen form Fig. 4.3 (d). This is further corroborated by studying the contour of reaction rate of HO_2 for case T4, the plot of which has not been shown. Smaller scales enhance the transport of species and mixing between the reactants, which in turn lead to the creation of pockets of flame around the reaction zone. The reaction rate is generally very high in these flame pockets, and this leads to the accelerated growth of the flame kernel and its surface area. This supports the previous observation of significantly higher values of integrated reaction rate and Lagrangian time derivative values of H_2O and HO_2, for case T4 at subsequent stages of kernel growth, in comparison with the other cases of turbulence and the laminar case.

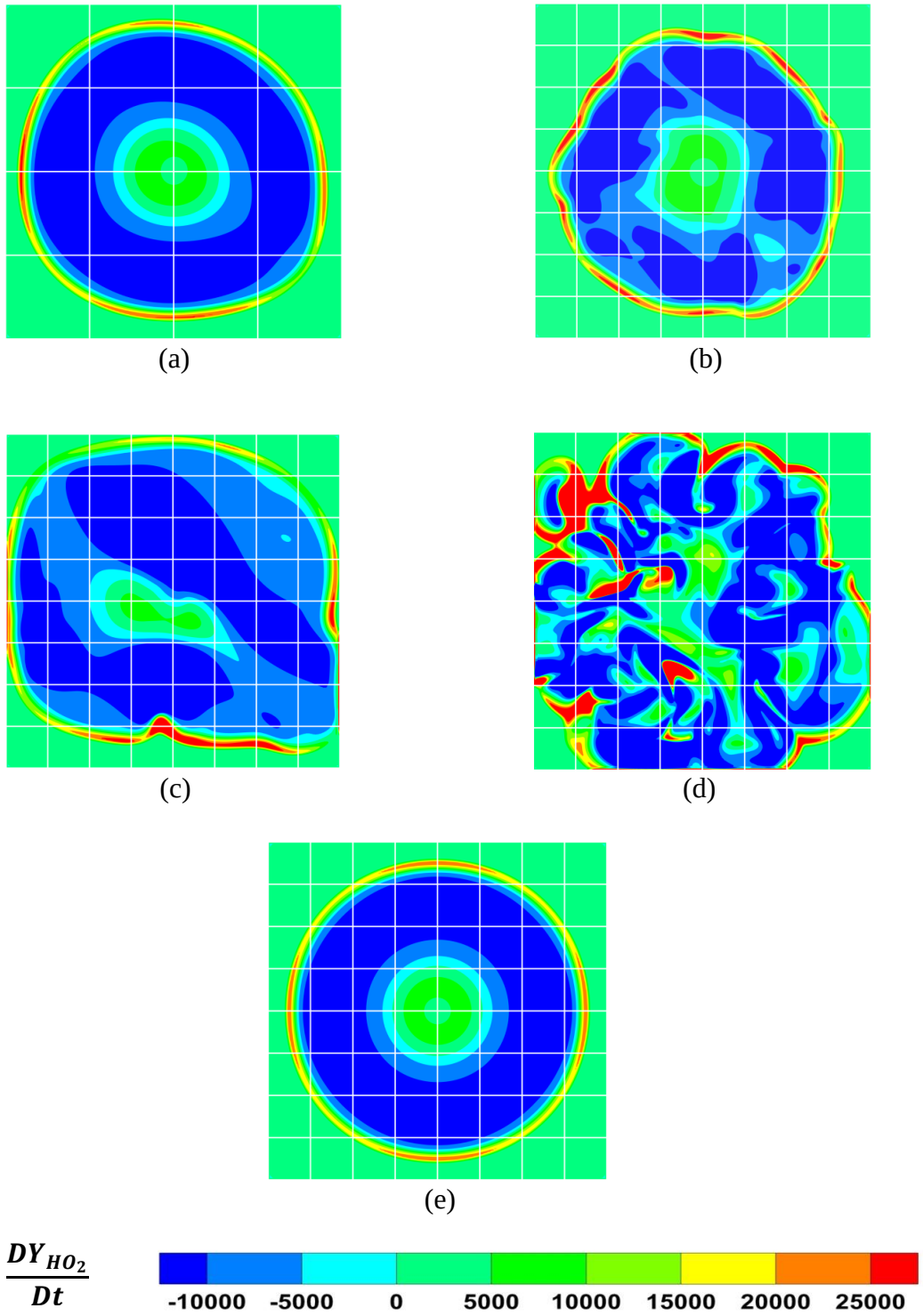

Figure 4.3: Lagrangian contours ($y - z$ plane) of HO_2 for (a) Case T1 (b) Case T2 (c) Case T3 (d) Case T4 and (e) Laminar Case, at t = 0.195 ms and x = 0 cm.

Contours of mass fraction of H_2O at the end of the run (t = 0.195 ms) for different test cases are given in Fig. 4.4. All the contours are views of y - z planes (1cm x 1 cm) at x = 0 cm. It can be observed that the flame growth is highest for case T4 followed by T3 and T2. This shows that turbulence length scale has a greater influence on flame chemistry and structure in comparison with turbulence intensity. Laminar flame is spherical and its size is comparable to case T1, since the parameters for case T1 are the closest to those for the laminar case. Contours of mass fractions of H for the different cases considered are shown in Fig. 4.5.

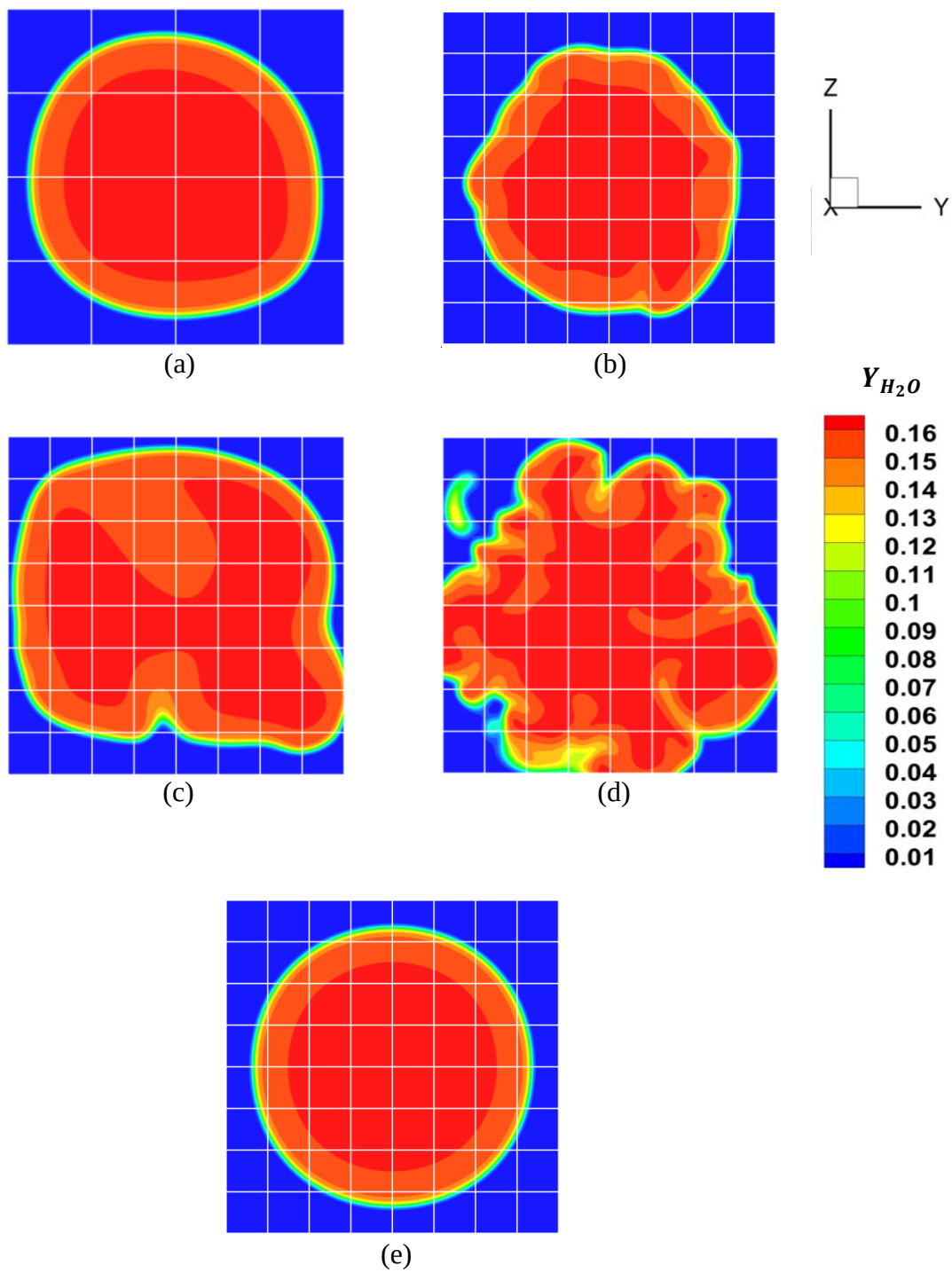

Figure 4.4: H_2O mass fraction contours ($y - z$ plane) for (a) Case T1 (b) Case T2 (c) Case T3 (d) Case T4 and (e) Laminar case, at t = 0.195 ms and x = 0 cm.

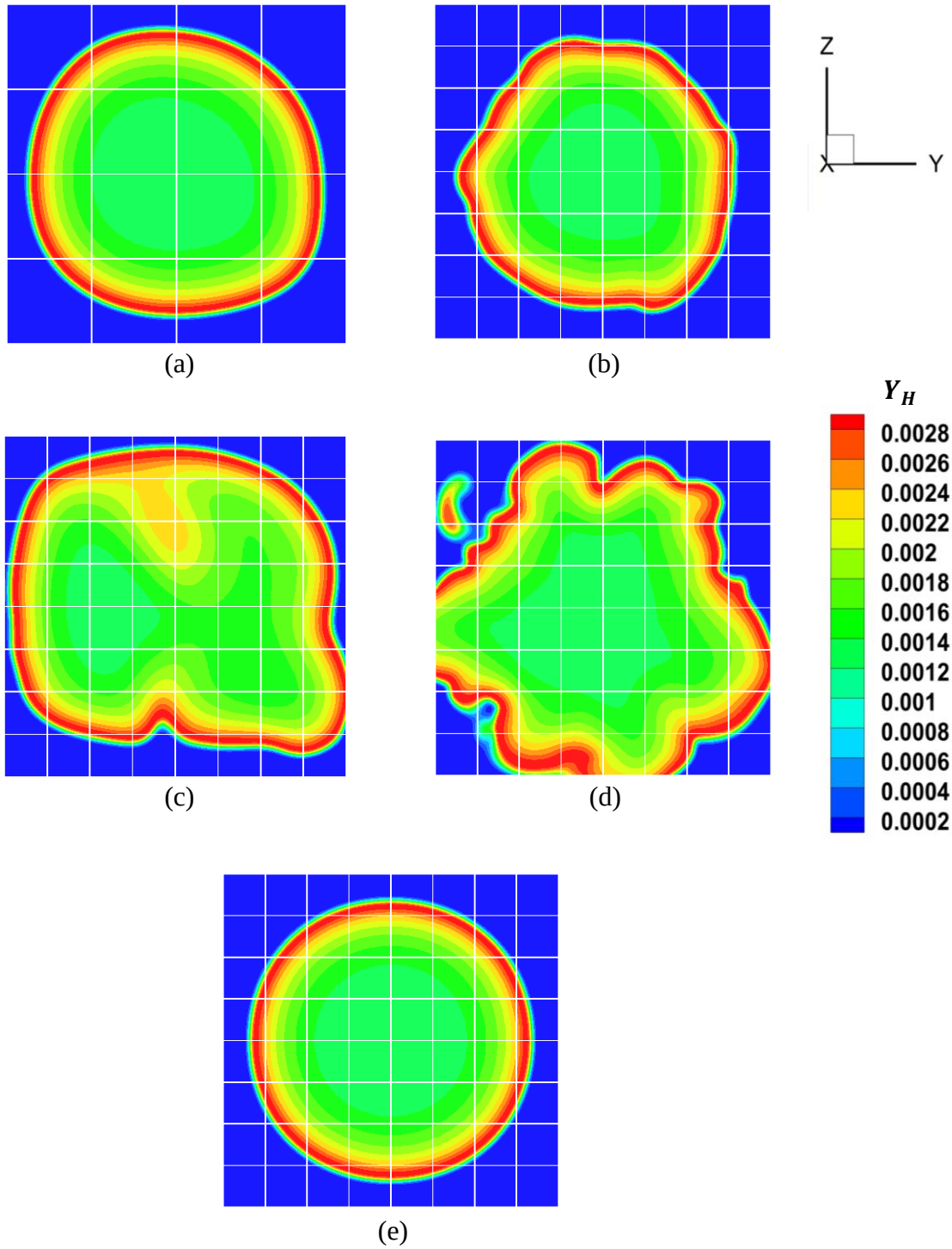

Figure 4.5: H mass fraction contours ($y - z$ plane) for (a) Case T1 (b) Case T2 (c) Case T3 (d) Case T4 and (e) Laminar Case , at t = 0.195 ms and x = 0 cm.

From Fig. 4.5, it is clear that H, being an intermediate specie, has higher values at the reaction zone, i.e., close to the surface of the flame, since it is primarily produced at the reaction zone. The extent to which the reaction zone is deformed is a measure of the amount of wrinkling that the flame surface has undergone. From the figure, it can be inferred that length-scales play a more significant role in the structure of the flame surface, in comparison with the intensity of turbulence. Some islands of higher H mass fractions are seen outside the flame surface, for case T4, as can be seen in Fig. 4.5 (d). Also, there is evidence of some surface extinction on the bottom right corner of the H mass fraction contour for case T4. Higher intensity of turbulence combined with a smaller characteristic length scale, thus can create regions of enhanced reaction rates and regions where there is extinction. With the increase in turbulence intensity, it is conjectured that instabilities in hydrogen combustion will occur.

Fig. 4.6 shows contours of mass fraction of HO_2 at t = 0.195 ms for different cases. It is evident from the figures that HO_2 is an indicator of the reaction zone. As observed for H, flame pockets are also observed for HO_2, in the case of smaller-scaled turbulence and more intense turbulence, i.e., T4. The other intermediates, namely, O and OH exhibit slightly different patterns. The trend of O is more or less similar to that of H, with differences in the thickness of the band of higher mass fraction observed at the flame surface. OH, on the other hand, matches H_2O in its trend. The contours of logarithmic temperature for the different cases are shown in Fig. 4.7.

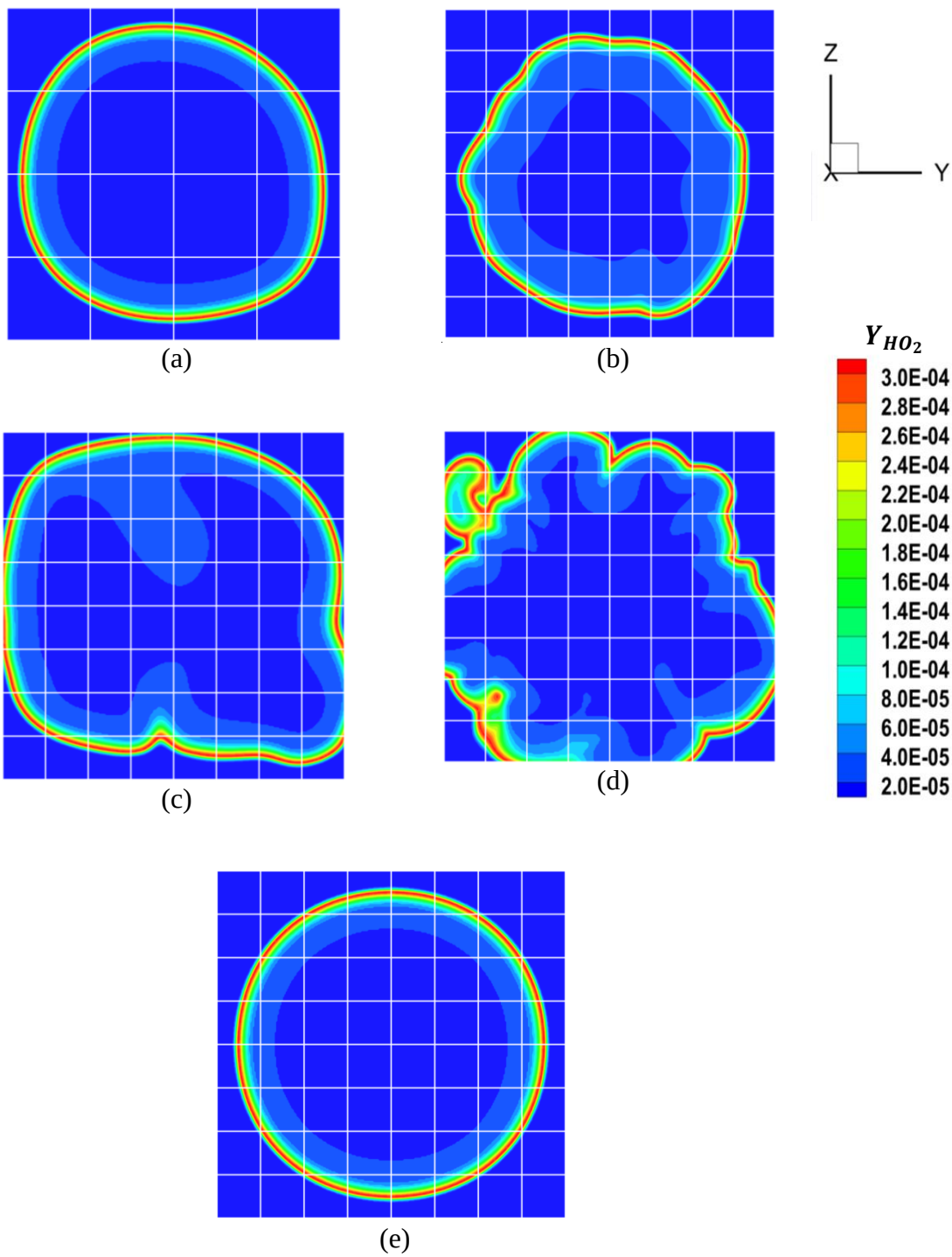

Figure 4.6: HO_2 mass fraction contours ($y - z$ plane) for (a) Case T1 (b) Case T2 (c) Case T3 (d) Case T4 and (e) Laminar case, at t = 0.195 ms and x = 0 cm.

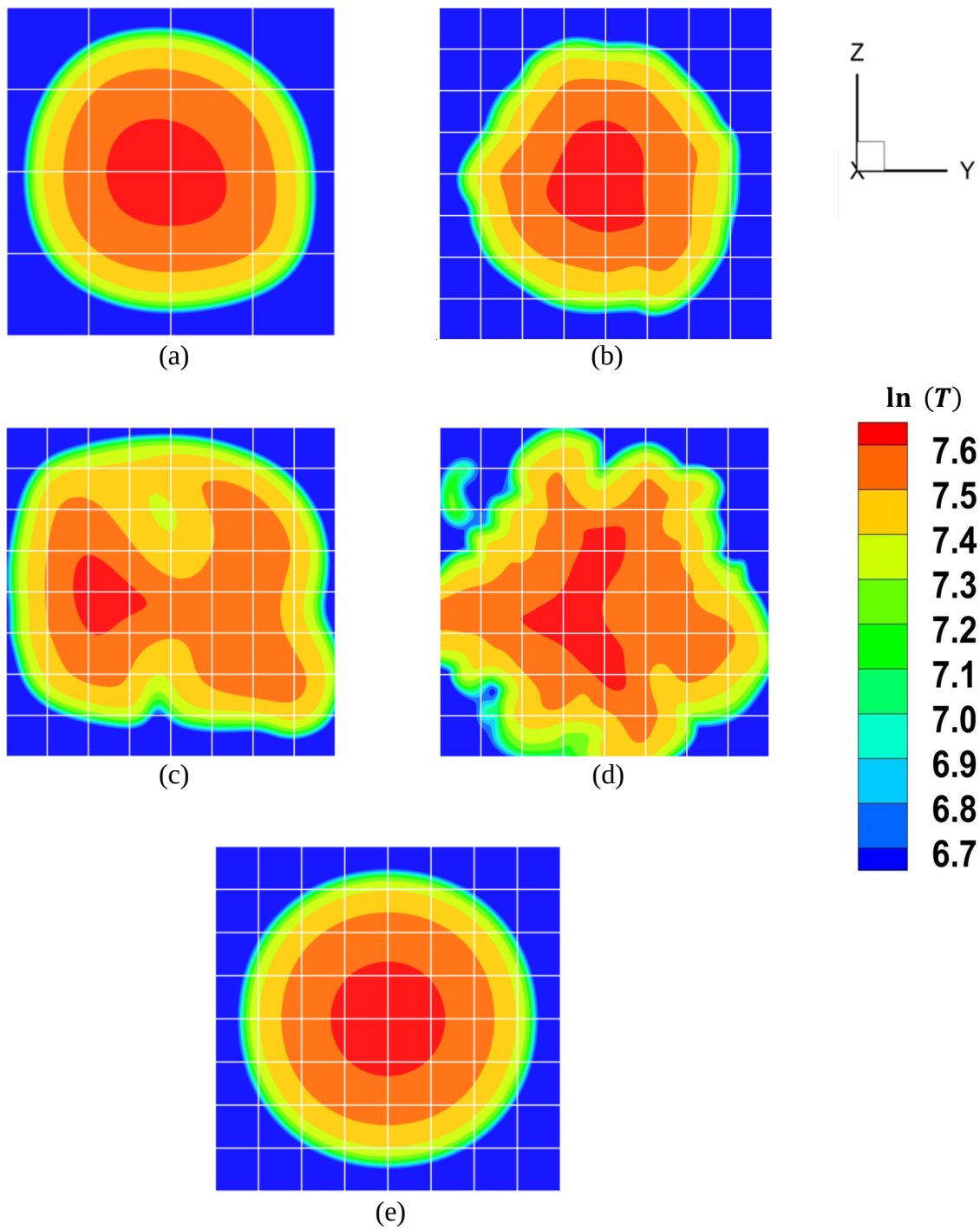

Figure 4.7: Temperature contours ($y - z$ plane) for (a) Case T1 (b) Case T2 (c) Case T3 (d) Case T4 and (e) Laminar case, at t = 0.195ms and x = 0cm.

From Fig. 4.7, it is evident that case T4 has an island of lower temperatures on the bottom right corner of the flame surface, as can be seen in Fig. 4.7 (d), which is an indication of surface extinction. Flame-pockets begin to emerge at small length scales and higher intensities of turbulence. This can be observed near the top left corner in 4.7 (d). From these observations, it can be inferred that the role of turbulence length scales is more significant in combustion chemistry and the nature of the flame surface, but turbulence intensity apparently plays a more significant role in deciding extinction and combustion instabilities.

Iso-surfaces of H_2O mass-fraction (Y_{H_2O}= 0.16) for different cases are given in Fig. 4.8. It is clear upon observation that the shape of the kernel for case T1 is almost similar to that of the laminar case. The changes in shape for larger length scales are broad and comparable to the size of the domain, whereas they are finer and more widespread for smaller length scales. Also, with increase in turbulence intensity, changes in the flame surface become more prominent. The highest wrinkling of the flame surface is observed for case T4.

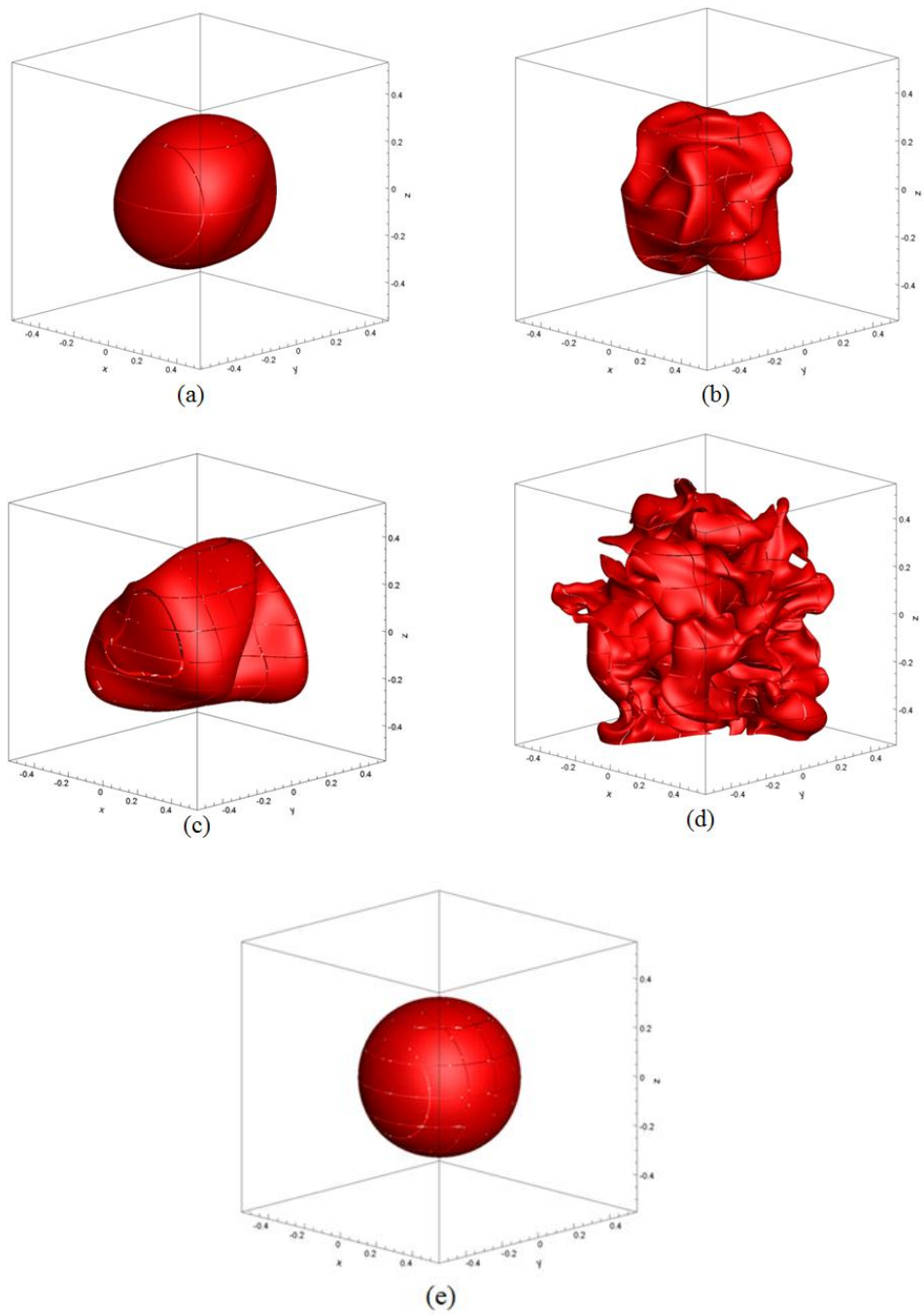

Figure 4.8: Iso-surfaces of H_2O (Y_{H_2O} = 0.16) for (a) Case T1 (b) Case T2 (c) Case T3 (d) Case T4 and (e) Laminar Case, at t = 0.195 ms.

4.2 Flame Surface, Curvature and Strain-rate Statistics

Curvature and strain rate pdfs are used to study the evolution of the flame kernel over time. A flame in a turbulent flow-field is subjected to curvature effects and tends to get strained. These factors decide the local structure of the flame surface and describe the departure from stable burning conditions [9]. Thus, studying the effects of turbulence on flame curvature and strain rate is important for combustion applications. Flame surface area evolution with time is also studied. Flame surface area is calculated at eight discrete points of time through the runs and a curve is fit. All the results in this section are obtained using the Anaflame package [9]. Flame surface area is calculated by discretizing the flame surface into triangular elements and summing up the areas of each of these triangles. The flame is identified by an iso-surface of temperature (T = 1400 K) for the calculation of flame surface area. The expressions used to calculate curvature and strain rates are given below,

- The tangential component of strain rate [9]

$$\epsilon_t = t_i t_j \frac{\partial u_i}{\partial x_j} \tag{4-1}$$

- The normal component of strain rate [9]

$$\epsilon_n = n_i n_j \frac{\partial u_i}{\partial x_j} \tag{4-2}$$

  where **n** and **t** are unit normal and tangential vectors to the flame front.

- The curvature of the flame front [9]

$$\nabla . n = -\left(\frac{1}{R_1} + \frac{1}{R_2}\right) \tag{4-3}$$

where $k_1=1/R_1$ and $k_2=1/R_2$ are the principal curvatures of the flame surface. They measure the highest curvature and the curvature in the perpendicular direction. Mean curvature is the arithmetic mean of the principal curvatures.

- Probability Density Function (pdf) [9]

$$P(a \leq U_i \leq b) = \int_a^b f(u_i) du_i \tag{4-4}$$

where a and b are the ends of the interval [a, b] in which the probability of finding the variable U_i is to be calculated.

The evolution of flame surface area with time is depicted in Fig. 4.9 (a). As can be seen from the figure, the growth of the flame surface is highest for case T4, followed by T3 and T2. This may be attributed to the fact that turbulence tends to enhance the surface area of the flame through wrinkling. This enhancement is stronger for smaller scaled-turbulence in comparison with that for higher intensity turbulence. The rapid increase of surface area for case T4 at later stages, in comparison with the other cases may be attributed to the formation of flame pockets with higher reaction rates, as discussed earlier. The surface area growth for the laminar case is apparently higher than that for case T1 initially, but the growth-rate of the kernel in case T1 is very close to that for the laminar case. This may be because case T1 has large-scaled turbulence with lower intensity of turbulence, making it closest to the laminar case among the four turbulence cases. In Fig. 4.9 (b), effective radius of the flame kernel is plotted against time. Effective radius (r_{eff}) is the radius that a sphere would have if its surface area were equal to the surface area of the kernel. It is calculated as given in Eq. 4.5.

$$r_{eff} = \sqrt{\frac{Flame\ surface\ area}{4\pi}} \tag{4-5}$$

The trend in Fig. 4.9 (b) is exactly similar to that in Fig. 4.10 (a), the only difference being that the curves rise at a slower rate, since $r_{eff} \alpha\ flame\ area^{\frac{1}{2}}$. It can be observed from the said figure that effective flame radius reaches a value that is greater than the size of the domain for cases T4 and T3 near the end of the runs. This means that if the kernel were spherical it would be larger than the domain under consideration. This shows the ability of turbulence to wrinkle the flame surface, due to non-uniform flow-field effects, and increase its surface area.

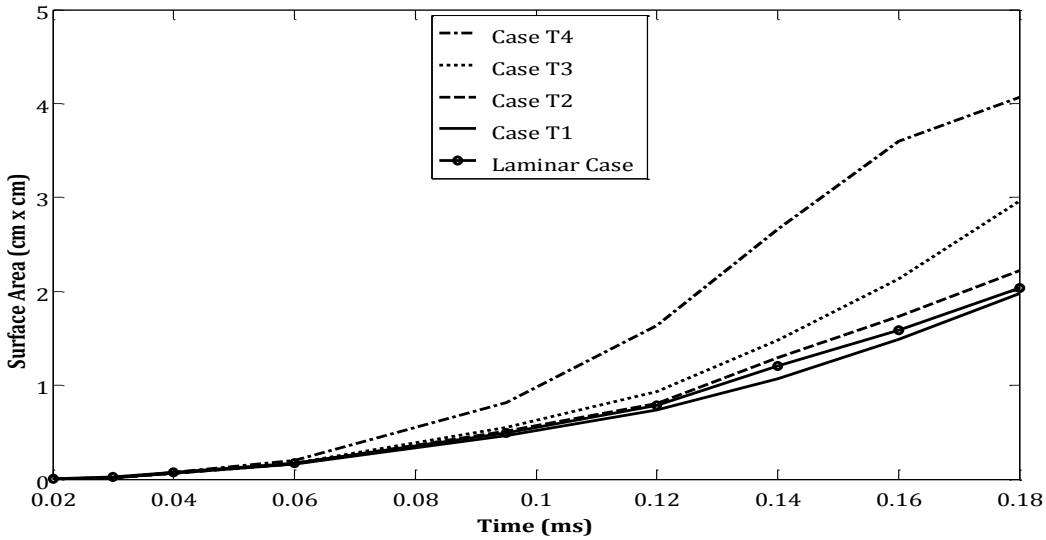

(a)

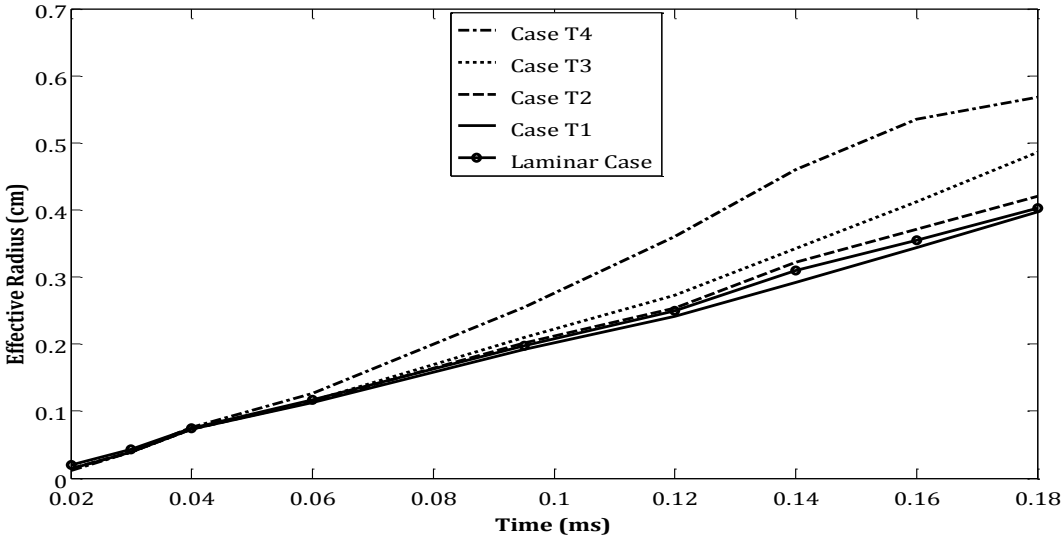

(b)

Figure 4.9: Evolution of (a) surface area of the flame and (b) effective radius (r_{eff}), with time, for different cases.

A comparison of pdfs of mean curvature for different cases is made in Fig. 4.10 at 4 different points of time. The kernel is initially spherical and is thus highly curved in all the cases. As time progresses, the kernel grows in size and becomes wrinkled. This makes the curvature pdf broader. From Fig. 4.10, it can be seen that the flame kernels in all the cases start out with a positive mean curvature and with time, the curvature pdfs travel left, become centered around zero and broaden. This is because with time and the effect of turbulence, curvatures tend to become negatively skewed. It is clear from the figures that the kernel in case T1 undergoes very little change in shape with time. The pdf of curvature for T1 is narrow and it undergoes very little broadening with time. However, it traverses from left to right towards zero. The peak of the pdf for case T1 is around 0.8. Also, the pdf curves exhibit more noise at the beginning, but eventually smoothen out. It can also be seen that the pdf curve of case T4 undergoes the highest broadening, followed by those for cases T2 and T3. This shows that length-scales have a greater influence on the mean curvature of a flame kernel in comparison with the intensity of turbulence. This supports the higher wrinkling for smaller length scales previously observed in Fig. 4.8. It can also be seen from the curvature plots that the pdf curve for case T3 has dual peaks for most part of the run. The secondary peak starts to disappear near the end of the run. This may indicate that the curvature changes caused by larger length scales resemble relatively large localized dents, instead of the widespread wrinkling patterns on the surface like those observed for cases T2 and T4.

Fig. 4.11 shows the pdfs of shapefactors for the different cases of turbulence. Shapefactor (S) is the ratio of the smaller principal curvature over the larger principal curvature (k_{small}/k_{large}). It takes values between -1 and 1, with S = -1 meaning the surface has

a saddle point, S = 0 meaning the surface is cylindrically curved and S = 1 meaning the surface is spherically curved. From Fig. 4.11, it is clear that larger-scaled turbulence, i.e., cases T1 and T3 have curvatures that are predominantly spherical or cylindrical, with very little probability of finding a saddle point on the flame surface. This strengthens the view that larger scales of turbulence do not have widespread wrinkling. Cases T2 and T4 however, have curves that are tending towards a Gaussian curve and are centered close to zero; this indicates higher and more widespread wrinkling.

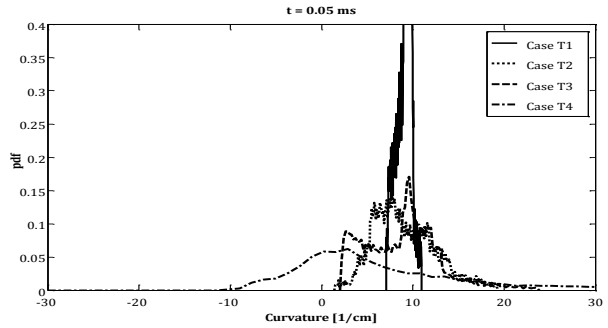

(a)

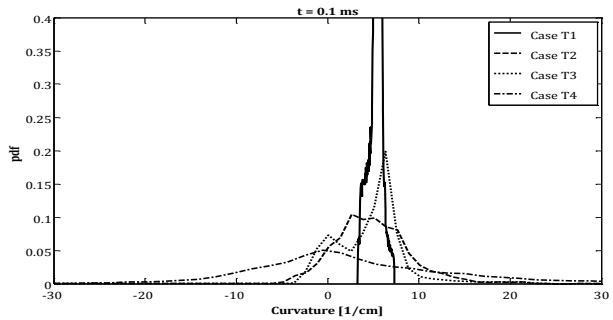

(b)

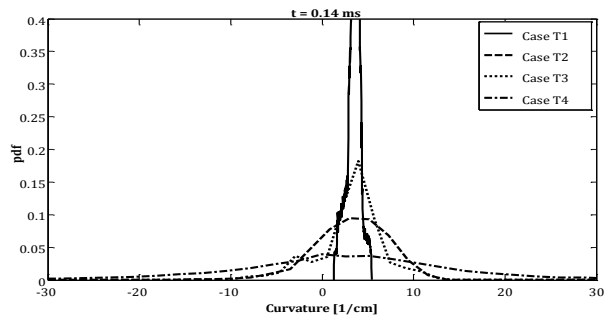

(c)

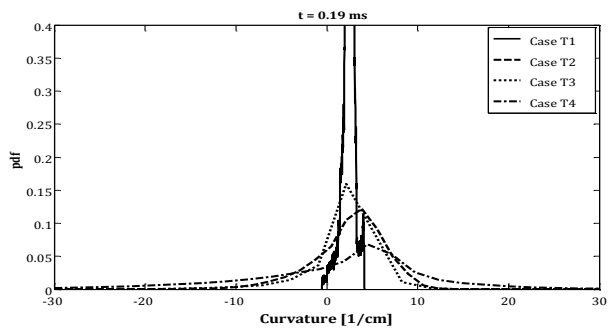

(d)

Figure 4.10: Comparison of pdfs of mean curvature for the different cases at (a) t = 0.05 ms (b) t = 0.1 ms (c) t = 0.14 ms (d) t = 0.19 ms.

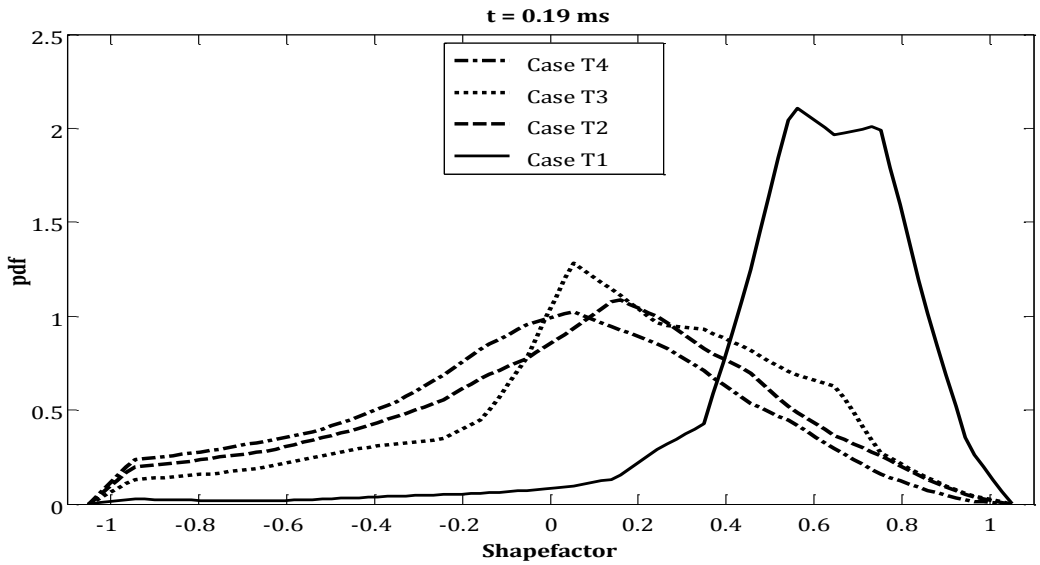

Figure 4.11: pdfs of shapefactor for the different cases of turbulence, at t = 0.19 ms.

Tangential strain rate pdfs for different cases are compared at 4 different points through the runs. The results are depicted in Fig. 4.12. All the curves appear to be centered around zero and broaden with time. It is observed that the pdf curve for case T1 stays so close to zero pdf line that it is almost invisible in comparison with the curves for other cases. This is probably due to the fact that the kernel in case T1 undergoes very little change in curvature because of the presence of larger length scales and lesser turbulence intensity, and thus is the least strained among all the cases. The pdf curve for case T4 broadens the most, indicating that higher straining. Cases T2 and T3 seem to have comparable effects on the tangential strain rate. As discussed earlier, strain is a result of the non-uniform nature of the turbulent flow-field. The effect of this non-uniformity apparently increases with the decrease in turbulence length scale and the increase in turbulence intensity, as can be seen in Fig. 4.12.

Length scales seem to play a more significant role in stretching and deforming the flame kernel, thus increasing the strain rates. Normal strain rate pdfs exhibit similar trends as their tangential counterparts.

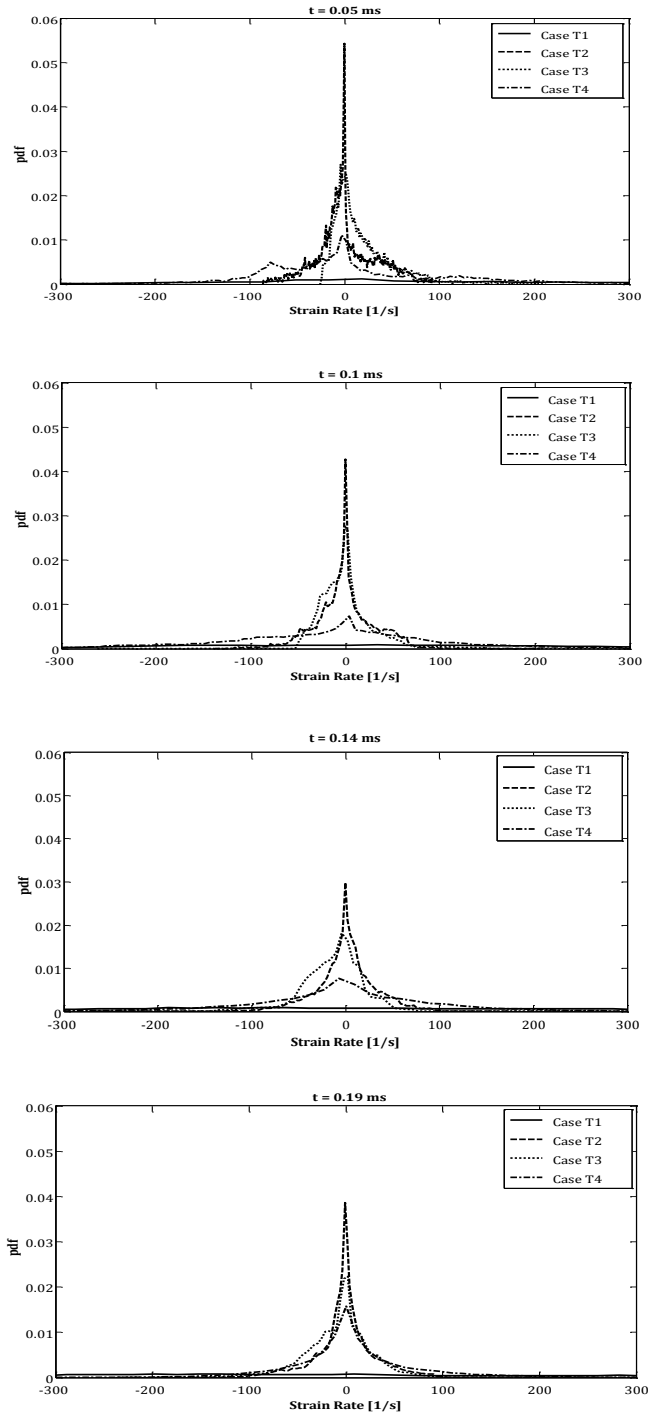

Figure 4.12: Comparison of pdfs of tangential strain rate for the different cases at (a) t = 0.05 ms (b) t = 0.1 ms (c) t = 0.14 ms (d) t = 0.19 ms.

4.3 Summary

It is observed that turbulence enhances the Lagrangian time derivative of H_2O. This enhancement increases with the decrease in turbulence length scale (L_T) and increase in turbulence intensity (U_{rms}/S_L). This shows the important role played by small-scale eddies in flame chemistry. The production rate of H_2O is enhanced to the highest extent in the case with the lowest length scale and the highest turbulence intensity. It is observed that the growth of the flame is highest for the case with the lowest L_T and the highest U_{rms}/S_L.

Further, it is observed that the role of U_{rms}/S_L is more significant in combustion chemistry and the nature of the flame surface, while L_T has a greater effect on extinction and flame-pocket formation in the flame. The changes in the shape of the flame are broader and comparable to the size of the domain for cases with larger L_T, whereas they are finer and more widespread for smaller length scales. The flame surface area growth is highest for the case with the lowest L_T and the highest U_{rms}/S_L. Case T1 and the laminar case have comparable surface areas. Similar trend is observed for effective radius of the flame (r_{eff}). Higher changes in curvature are observed for cases with lower L_T and higher values of U_{rms}/S_L. Length scales play a more significant role in stretching and deforming the flame kernel. Thus, the highest strain rates are observed for cases with lower values of L_T.

CHAPTER 5

Summary and Conclusions

In this chapter, results from the present work are summarized and recommendations for future studies are proposed.

5.1 Concluding Remarks

In this study, the role of turbulence conditions on the initial and subsequent stages of premixed flame kernel formation during combustion of a stoichiometric mixture of hydrogen and air is studied using DNS. The results from these runs are compared with a reference case with laminar conditions. Two different turbulence intensities and two different characteristic length scales are varied to achieve four different turbulence conditions. Results from these runs are discussed at two main stages of kernel development: a) initial stages of the kernel, and b) the subsequent evolution of the premixed flame kernel. Conclusions drawn by observing results from (a) and (b) are discussed in the following sections.

5.1.1 Initial stages of kernel development

In this section, results from pre-ignition and times close to ignition of the hydrogen-air mixture are summarized. It is observed that the effect of turbulence on ignition delay depends on the kind of turbulence conditions under consideration. Turbulence may expedite or delay the process of ignition, in comparison with the laminar case, depending on the values of parameters deciding the type of turbulence. Ignition delay is observed for case T4, whereas

cases T1, T2 and T3 observe ignition at almost the same time as the mixture in the laminar case ignites. This indicates the smaller-scaled and more intense turbulence slightly delays the onset of ignition and initially inhibits the kernel growth. However, the difference in ignition delays is only about 1 μs, and so, these observations cannot be generalized. The integrated reaction rate for H_2O is almost similar for the different cases considered for the first 40-60 μs of kernel growth, but beyond that point, the highest values of the integrated reaction rates are observed for case T4, followed by those for cases T3, T2, T1 and the laminar case.

The integrated reaction rate of HO_2 is highest for case T4, followed by T3, T2, T1 and the laminar cases, beyond t = 0.060 ms, which is similar to the trend exhibited by H_2O. There are no appreciable differences in the values of the integrated Lagrangian time derivative of H_2O and HO_2, for the first 40-60 μs, but beyond that point, smaller-scaled and more intense turbulence tends to enhance the reaction rate of H_2O and HO_2 and in turn increase the values of the Lagrangian time derivatives for cases T4 and T3 relative to the other cases.

The most significant change in kernel shape during the early stages of kernel growth is observed for case T4, followed by cases T3, T2 and T1. The flame surface area and effective radius of the kernel are initially highest for the laminar case and lowest for case T4, but kernels in cases with turbulence tend towards higher surface area at subsequent stages of kernel growth; showing the ability of turbulent length scales to enhance the surface area of the kernel.

5.1.2 Subsequent stages of flame kernel evolution

In this section, results from stages that are post-ignition are discussed. The studies focus on a flame kernel that is fully developed or close to being fully developed. It is found that the integrated values of Lagrangian time derivatives and reaction rates for H_2O are highest for case T4, followed by T3, T2, T1 and laminar cases. Contours of Lagrangian time derivative of HO_2 show the presence of flame pockets, which are islands of higher mass fraction for case T4, showing the ability of the smaller scales to enhance species transport and mixing. Similar trend is observed for intermediates, H, O and OH. The flame growth is highest for case T4, followed by cases T3, T2, laminar and T1. Higher wrinkling of the flame surface was observed for cases with smaller-scaled turbulence. Also, flame pockets begin to appear for cases with smaller scales and more intense turbulence.

The flame surface area, near the end of the run, is highest for case T4, followed by that for cases T3, T2, T1 and the laminar case. A characteristic of turbulence is the presence of non-uniform flow effects. This subjects the flame to curvature effects and straining. Evolution of mean curvature and tangential strain rate pdfs is studied for different cases. It is observed that the cases with lower length scales have higher and more widespread changes in curvature, because of higher wrinkling.

5.2 Recommendations for Future Work

The current study focuses on the stages in the formation and development of a premixed flame kernel during the combustion of a stoichiometric hydrogen-air mixture under turbulent

conditions. This represents a narrow but relevant part in the study of turbulent combustion of hydrogen in air. This study can be improved in the following ways:

i. The current study uses a stoichiometric mixture of hydrogen and air. It will be interesting to conduct the same study with different equivalence ratios, and observe the difference in results for leaner and richer mixtures and the case with unity equivalence ratio.

ii. This study can be further strengthened by considering more cases of turbulence, say nine or sixteen cases, as against the current value of four. This will result in a clearer idea of the effects of various parameters of turbulence on flame chemistry and structure.

iii. The current study uses a reduced six-step reaction mechanism for hydrogen-air combustion. A more complex reaction mechanism can be used to improve the accuracy of some of the predictions made and conclusions drawn in this study.

iv. Cases with mean flow in one particular direction, along with turbulence, can be considered, and results from these cases can be compared with those from cases with isotropic turbulence. This will help in the study of the effects of mean flow on flame structure, reaction chemistry and the possibility of extinction in parts of the flame.

v. The study can be extrapolated to include more than one fuel in the mixture, say CH_4, along with H_2. This will aid in the comparison of chemistry and flame surface statistics for the different species for the same turbulence conditions, which in turn will show the difference in effects of turbulent conditions on combustion of different species.

REFERENCES

[1] N. Babkovskaia, N.E.L. Haugen, and A. Brandenburg. "A high-order public domain code for direct numerical simulations of turbulent combustion." *Journal of Computational Physics,* pp. 230:1-12, 2011.

[2] M. Baum, T.J. Poinsot, D. Hayworth, and N. Darabiha. "Direct numerical simulation of H2/O2/N2 flames with complex chemistry in two-dimensional turbulent flows." *Journal of Fluid Mechanics,* pp. 281:1-32, 1994.

[3] H. Wang, K. Luo, S. Lu, and J. Fan. "Direct numerical simulation and analysis of a hydrogen/air swirling premixed flame in a micro cumbustor." *Interntational Journal of Hydrogen Energy,* pp. 36:13838-13849, 2011.

[4] H. Wang, K. Luo, K. Qiu, S. Lu, and J. Fan. "A DNS study of hydrogen/air swirling premixed flames with different equivalence ratios." *International Journal of Hydrogen Energy,* pp. 37:5246-5256, 2012.

[5] T. Baritaud, T. Poinsot, and M. Baum. "Direct numerical simulation for turbulent reacting flows." *Éditions Technip, Paris,*1996.

[6] T. Echekki, T.J. Poinsot, T. Baritaud, and M. Baum. "Modeling and simulation of turbulent flame kernel evolution." *8th International Symposium on Transport Processes in Combustion, San Francisco,* 1995.

[7] N. Vasudeo, T. Echekki, M.S. Day, and J.B. Bell. "The regime diagram for premixd flame kernel-vortex interactions-Revisited." *Physics of Fluids,* pp. 22, 043602:1-10, 2010.

[8] P.E. Hamlington, A.Y. Poludnenko, and E.S. Oran. "Interactions between turbulence and flames in premixed reacting flows." *Physics of Fluids,* pp. 23, 125111:1-19, 2011.

[9] C. Zistl, R. Hilbert, G. Janiga, and D. Thévenin. "Increasing the effeciency of postprocessing for turbulent reacting flows." *Computing and Visualization in Science,* pp. 12:383-395, 2009.

[11] D. Thevénin, O. Gicuel, J. De Charentenay, R. Hilbert, and D. Veynante. "Two- versus three-dimensional direct simulations of turbulent methane flame kernels using realistic chemistry." *Proceedings of the Combustion Institute*, Volume 29, pp. 2031-2039, 2002.

[12] C.F. Kaminski, X.S. Bai, J.Hult, A. Dreizler, S. Lindenmaier, and L. Fuchs. "Flame growth and wrinkling in a turbulent flow." *Applied Physics B*, Volume 71, pp. 711-716, 2000.

[13] K.W. Jenkins and R. S. Cant. "Curvature effects on flame kernels in a turbulent environment." *Proceedings of the Combustion Institute*, Volume 29, pp. 2023-2029, 2002.

[14] T.D. Dustan and K.W. Jenkins. "Flame surface density distribution in turbulent flame kernels during the early stages of growth." *Proceedings of the Combustion Institute*, Volume 32, pp. 1427-1434, 2009.

[15] Marc Lange. "Investigation of turbulent flame kernels using DNS on clusters." *Proceedings of the 5th International Conference on High Performance Computing for Computational Science*, pp. 24-38, 2003.

[16] S. Gaashi, J. Hult, K.W. Jenkins, N. Chakraborty, S. Cant, and C.F. Kaminski. "Curvature and wrinkling of premixed flame kernels-comparisons of OH PLIF and DNS data." *Proceedings of the Combustion Institute*, Volume 30, pp. 809-817, 2005.

[17] M. Klein, N. Chakraborty, and R.S. Cant. "Effects of turbulence on self-sustained combustion in premixed flame kernels: A Direct Numerical Simulation (DNS) study." *Flow Turbulence Combustion*, Volume 81, pp. 583-607, 2008.

[18] H. Shalaby and D. Thevénin. "Statistically significant results for the propagation of a turbulent flame kernel using direct numerical simulation." *Flow Turbulence Combustion*, Volume 84, pp. 357-367, 2010.

[19] N. Chakraborty, J.W. Rogerson, and N. Swaminathan. "The scalar gradient alignment statistics of flame kernels and its modeling implications for turbulent premixed combustion." Volume 85, pp. 25-55, 2010.

[21] J. Ströhle and T. Myhrvold. "An evaluation of detailed reaction mechanisms for hydrogen combustion under gas turbine conditions." *International Journal of Hydrogen Energy*, Volume 32:1, pp. 125-135, 2007.

[22] J. Li, Z. Zhao, A. Kazakov, and F.L. Dryer. "An updated comprehensive kinetic model of hydrogen combustion." *International Journal of Chemical Kinetics*, Volume 36:10, pp. 566-575, 2004.

[23] J.H. Williamson. "Low-storage Runge-Kutta schemes." *Journal of Computational Physics*, 35, pp. 48-56, 1980.

[24] T. Poinsot and S. Lele. "Boundary conditions for direct simulations of compressible reacting flows." *Journal of Computational Physics*, 101, 1, pp. 104-129, 1992.

[25] J.T. Jensen, N.E.L. Haugen and N. Babkovskaia. "Calculation of the minimum ignition energy based on the ignition delay time." *Preprint submitted to Combustion and Flame*, Oct. 6th, 2011.

[26] P. A. Libby. "Introduction to Turbulence." Taylor and Francis, 1989.

[27] P.H. Alfredsson, A. Hanifi, A.V. Johansson, and D.S. Henningson. "Transition, Turbulence and Combustion Modeling." *Lecture Notes from the 2nd ERCOFTAC Summerschool held in Stockholm 10-16 June, 1998.* Kluwer Academic Publishers, 1999.

[28] L. Vervisch, D. Veynante, and J.P.A.J. van Beeck. "Turbulent Combustion." *Lecture Series from von Karman Institute for Fluid Dynamics, Belgium, 2009-07.* VKI LS, 2009.

[29] T. Echekki, T. Poinsot, T. Baritaud, and A. Trouve. "Modélisation et simulation numérique directe de l'allumage d'une flamme turbulente." *Rapport 41 525-Août 1994-10.* Institut Français du Pétrole, 1994.

[30] Markus Baum. "Etude de l'allumage et de la structure des flammes turbulentes." PhD thesis, Ecole Centrale Paris, 1994.

[31] K. Kuo. "Principles of Combustion." John Wiley and Sons, 1986.